frontiers | Frontiers in Energy Research

TYPE Original Research
PUBLISHED 13 September 2024
DOI 10.3389/fenrg.2024.1454275

OPEN ACCESS

EDITED BY
Milad Shadman,
Federal University of Rio de Janeiro, Brazil

REVIEWED BY
Luiz Paulo De Freitas Assad,
Federal University of Rio de Janeiro, Brazil
Raad Qassim,
Federal Rural University of Rio de Janeiro, Brazil

*CORRESPONDENCE
Manuel Corrales-Gonzalez,
manuelalejandro.corralesgonzlez@edu.unige.it

RECEIVED 24 June 2024
ACCEPTED 26 August 2024
PUBLISHED 13 September 2024

CITATION
Corrales-Gonzalez M, Lavidas G, Lira-Loarca A and Besio G (2024) Wave energy assessment and wave converter applicability at the Pacific coast of Central America. *Front. Energy Res.* 12:1454275. doi: 10.3389/fenrg.2024.1454275

Wave energy assessment and wave converter applicability at the Pacific coast of Central America

Manuel Corrales-Gonzalez[1]*, George Lavidas[2], Andrea Lira-Loarca[1] and Giovanni Besio[1]

[1]Department of Civil, Chemical and Environmental Engineering, University of Genoa, Genoa, Italy, [2]Department of Hydraulic Engineering, Faculty Civil Engineering and Geosciences, Delft University of Technology, Delft, Netherlands

Nowadays, numerous governments have instituted diverse regulatory frameworks aimed at fostering the assimilation of sustainable energy sources characterized by reduced environmental footprints. Solar, wind, geothermal, and ocean energies were subject to extensive scrutiny, owing to their ecological merits. However, these sources exhibit pronounced temporal fluctuations. Notably, ocean dynamics offer vast energy reservoirs, with oceanic waves containing significant amounts of energy. In the Central American Pacific context, the exploration of wave energy resources is currently underway. Accurate numerical wave models are required for applied studies such as those focused on the estimation of exploitable wave power; and even more so in Central American region of the Pacific Ocean where existing numerical models simulations have so far relied on coarse resolution and limited validation field data. This work presents a high-resolution unstructured wave hindcast over the Central American Pacific region, implemented using the third-generation spectral wave model WAVEWATCH III over the period between 1979 and 2021. The results of the significant wave height have been bias-corrected on the basis of satellite information spanning 2005 to 2015, and further validation was performed using wave buoy and acoustic Doppler current profiler (ADCP) records located in the nearshore region of the Central America Pacific coast. After correction and validation of the wave hindcast, we employed the dataset for the evaluation and assessment of wave energy and its possible exploitation using different wave energy converters (WECs). This evaluation addressed the need to diverse the energy portfolio within the exclusive economic zones of Guatemala, El Salvador, Honduras, Nicaragua, Costa Rica, Panama, Colombia, and Ecuador in a sustainable manner. Moreover, a comprehensive analysis was carried out on the advantages of harnessing wave energy, juxtaposed with the imperative of regulatory frameworks and the current dearth of economic and environmental guidelines requisite for development within the region.

KEYWORDS

Pacific Ocean, wave climate, wavewatch III, marine renewable energy, wave energy converter, capacity factor, selection index for wave energy deployment

1 Introduction

In recent years, oceans have captured global attention due to changes and threats affecting marine life and coastal socio-economic activities. The need for understanding these changes and the development of resilient measures have become the starting point for developing predictive models with increasingly novel techniques. In addition, the recent world geopolitical situation in terms of energy supply to societies (Boungou and Yatié, 2022; Wan et al., 2023) has had important impacts on the energy market, which has given priority to the exploration of diverse energy sources to enhance energy security and maximize the usage of the energy mix with special attention to renewable resources (Decastro et al., 2024; UN, 2022).

One of the most untapped sources of renewable energies, despite their high and renewable energetic content, are those related to the ocean, i.e., marine energies. There are different ways to take advantage of marine renewable energy (MRE): wave energy, tidal energy, salinity gradients, and ocean thermal conversion (Kumar et al., 2022). The exploitation of MRE depends on the geographical location and metocean conditions, as well as the regulations chiefly on marine spatial planning and environment policies (Freeman et al., 2024; Salvador and Ribeiro, 2023; Soukissian et al., 2023; Ferrari et al., 2020). Moreover, wave energy technologies, as the rest of MRE, are mostly at the stages of its development, seeking to refine such technologies, understand and quantify the uncertainties associated with implementing energy conversion devices, and project economically feasible maintenance and operational conditions for wave energy converters (WECs) (Vieira et al., 2024).

Waves contain a substantial amount of energy, conservatively 3–5 times higher than wind energy (Waters, 2008); specifically, the wind gravity wave component, characterized by periods between 5 and 20 s, presents the highest energetic content (Holthuijsen, 2010) with respect to other oscillatory phenomena present in the ocean. A significant advantage of the exploitation of wave energy, similar to other marine energies from currents, saline gradients, or wind and solar radiation, is that wave energy can be estimated using wave hindcast (for historical and hence statistical analysis) and forecast models (for operational conditions at the short term and long-period changes for climate projections, for example) (Lehmann et al., 2017; Tawn and Browell, 2022).

Additionally, wave energy assessment has been developed traditionally on the basis of numerical models at different scales; some researchers employed global simulations, which provide comprehensive analysis across the whole globe but with a relatively coarse resolution (Gunn and Stock-Williams, 2012; Cornett, 2008). On the other hand, in order to develop site-specific analysis, simulations should be carried out at a high resolution, either in space or time. These types of analyses are usually developed for regional areas, such as the Mediterranean Sea (Lavidas and Venugopal, 2017a; b; Dialyna and Tsoutsos, 2021; Amarouche et al., 2020; Foteinis, 2022; Rasool et al., 2022), the Baltic Sea (Soomere and Eelsalu, 2014), the Indian Sea (Kumar and Anoop, 2015; Amrutha and Kumar, 2019), the South Pacific Ocean (Liu et al., 2023; Medina et al., 2023), the South China Sea (Kamranzad and Lin, 2020), and the Pacific nearshore regions of the American continent (Gorr-Pozzi et al., 2021; Ventura et al., 2022; Mediavilla and Sepúlveda, 2016; Lucero et al., 2017; Contestabile et al., 2015; Mazzaretto et al., 2020; Rusu and Onea, 2017). Despite previous studies in America evaluating wave power, none of them have evaluated WEC performance in the Central American Pacific region.

Regional wave energy evaluations have been developed using the wave numerical models, which provide wave integral parameters useful for such assessments. Several wave numerical models exist for the Pacific nearshore regions of the American continent. Examples include the early wave databases generated along the Chilean coasts by Fournier et al. (2004) and later by Beyá et al. (2017), as well as the wave database produced a 10-year worldwide wave hindcast (Arinaga and Cheung, 2012), using the WAVEWATCH III model. In addition, global wave hindcast and forecast data are available, most of which are openly accessible over the Pacific Ocean and specifically in the Central America region (NWS-NOAA, 2021; CMEMS, 2021; Perez et al., 2017). The wave databases generated for these specific regions were validated with few wave records due to the scarcity of measured wave data. The wave hindcast databases developed for the Pacific region of the American continent are listed in Table 1.

Models such as those used by NWS-NOAA (2021) and CMEMS (2021) use data assimilation, which improves accuracy by integrating satellite data, compensating for the lack of *in situ* measurements and increasing the reliability of the models in remote areas, mainly in regions with poor observational coverage.

The analysis of wave energy assessments present in the literature suggests that lower potential wave energy is present in lower latitude regions (Rusu and Onea, 2017), wherein the wave energy extracted can be feasible if WECs are designed or adapted to such wave climates (Bozzi et al., 2018). In addition, the distribution of wave climates around the world has shown a high percentage of swells approaching the Pacific coasts of Central America, according to Mazzaretto and Menendez (2024). This is due to the predominant wind action in the high-latitude regions, and the wave propagates toward the lower latitudes.

Although several investigations have shown that marine regions at high latitudes offer greater wave energy potential averaged over time than the intertropical regions, the energy density cannot be extracted constantly throughout the year due to seasonality, and extreme events pose challenges in terms of survivability and durability of the wave energy conversion devices. These factors make inter tropical regions attractive, where the amount of wave energy potential is not high but is more constant over time and less destructive for the devices (milder extreme conditions) (Martinez and Iglesias, 2020; Portilla-Yandun and Guachamin-Acero, 2023).

The development of marine energy exploitation projects still lacks a detailed and sound analysis of the specific devices. In particular, for wave energy exploitation, there is no well-established technology that could be adopted worldwide because wave climate is significantly different across locations spread worldwide This shortcoming justifies the development of the present research dedicated to exploring and implementing a detailed wave energy assessment through high-resolution numerical models and the analysis of possible wave energy conversion in the Pacific Ocean of Central America compared to other regions of the world. Furthermore, the efficiency of wave energy converters depends on their sizes, location, and the PTO design, coupled with the metocean conditions of the specific sites (Aderinto and Li, 2019;

TABLE 1 Numerical wave models generated onto the Pacific coast of Central America.

Model	Time coverage	Forcing	Time resolution	Spatial resolution	Bathymetry	Reference
EMC WIII global wave model Multi-1	1979 onward	CFSR and CFSRv2	3-hourly	Structured grid, 0.5°	GEBCO (30-min) LLCM (2020)	Chawla et al. (2009); Saha et al. (2014)
GOW2	1979 onward	CFSR and CFSRv2	Hourly	Higher-resolution structured grid, 0.25°	ETOPO2 v.2 Center (2006)	Perez et al. (2017)
Chilean Wave Atlas database	1979–2015	ERA-Interim, CFSR and CFSRv2	Hourly	Structured grid, 1°	ETOPO2 v.2	Beyá et al. (2017)
Multi-scale global hindcast	1994–2012	CFSR, CFSRv2, ECMWF (ECMWF, 2023)	3-hourly	Structured grid, 0.5°	ETOPO2 v2	Rascle and Ardhuin (2013)
WAVERYS	1993–2019	ERA5 ECMWF (Hersbach et al., 2020)	3-hourly	Structured grid, 0.2°	ETOPO2 v.2	Law-Chune et al. (2021)

Bozzi et al., 2014). In order to couple the information about the wave resource and different wave energy converters, several indices have been proposed. The development of different indices has been justified mainly because the different indicators have been developed taking into account different aspects related to the resource, the device, and a combination of the former two and economic aspects (Martinez and Iglesias, 2020; Lavidas, 2020). Research and development methodologies such as those described by Cruz et al. (2010), along with numerical models (Raghavan et al., 2024), are employed for the design of wave energy exploitation technologies, considering device dynamics and its interaction with the waves. Other approaches allow instead the evaluation of scaling through the Froude similarity law, adapting pre-existing converters to given wave conditions based on power matrices, for example, as performed by Lin et al. (2024) or Martić et al. (2024).

The present study aims to develop a detailed and reliable analysis of possible wave energy exploitation along the Pacific coast of Central America. The objective is intended to be achieved by the development and implementation of a new unstructured wave hindcast over the Pacific Ocean with a higher spatial resolution over the Pacific coast of Central America, reaching 1 km resolution in space along the shorelines and a time resolution of 1 h over the entire simulation period. The hindcast is then adjusted and optimized on the basis of satellite records over the Central American region. Hence, validation is performed using nearshore observation located along the Pacific coast of Central America. Wave climate obtained by this modeling approach is then employed for a pioneering evaluation of nine WECs located in 16 specific sites located near the coast of different countries in the target region. Analyses of the performances of the devices tailored for the specific wave climate of the different locations and cascade effects on possible environmental positive impacts (due to the substitution of energy sources, from non-renewable to renewable) are then presented.

The remainder of this paper is structured as follows: Section 2 presents the methodology used for the wave hindcast and wave energy assessment. Section 3 presents the main results and discussion, and finally, Section 4 presents the final remarks.

2 Materials and methods

A wave modeling optimization method has been developed for fulfilling the wave data requirements focused over the Central American Pacific Ocean. Simulations performed by a third-generation wave spectral model allow us to estimate the wave integral parameters and, subsequently, perform the model calibration, followed by a model correction procedure; finally, the model validation has been performed employing data from the nearshore region. Thereafter, a wave power potential assessment was performed, followed by the evaluation of nine floating body WECs over the studied region, based on the corrected and validated wave database generated in the previous step. These two stages of the methodology procedure are detailed in Sections 2.1, 2.2, respectively.

2.1 Wave hindcast

The spectral wave model WAVEWATCH III (hereinafter WWIII) version 6.07 (Björkqvist et al., 2020; Tolman et al., 2009) has been employed to implement a wide wave hindcast for the whole Pacific region, making use of an unstructured triangular mesh over the whole Pacific Ocean. The resolution of the mesh increases over the Central America Pacific region delimited by the latitudes −4° and 14° and longitudes between −92.7° and −76.6° (see Figure 1). Numerical modeling was conducted using an implicit numeric scheme, with previous tests evaluating mesh resolution and time steps. The mesh triangulation methodology employed in this study employed the Delaunay enhanced refinement technique presented by Engwirda (2014). The entire Pacific Ocean basin was considered in order to obtain the wave conditions developed in the

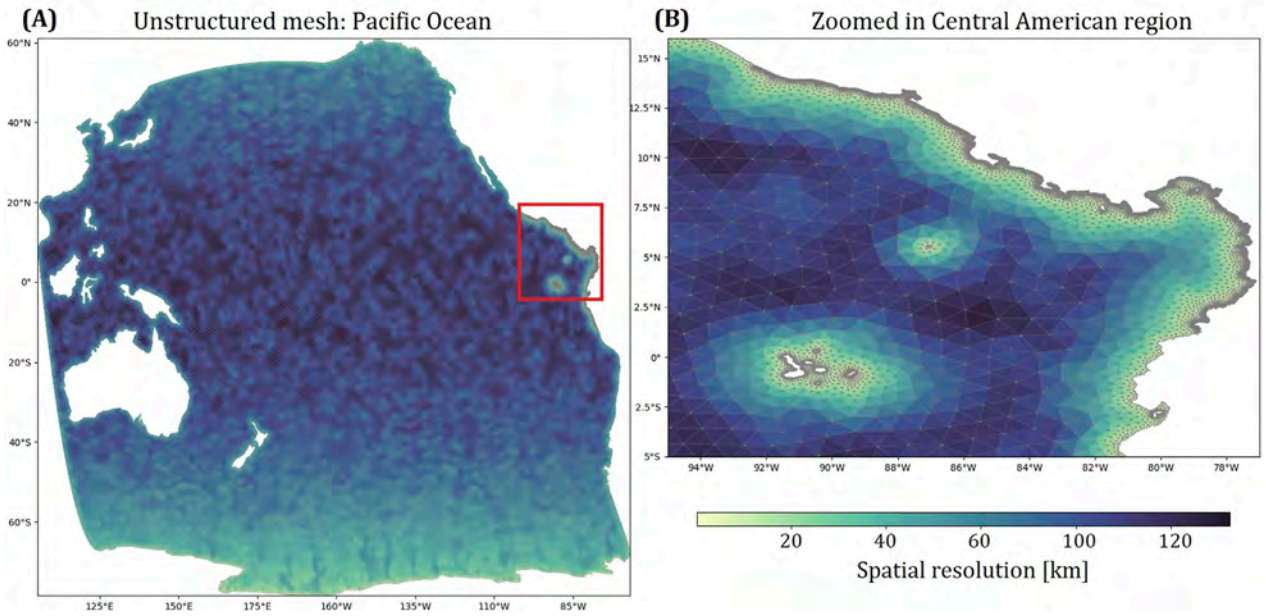

FIGURE 1
Unstructured mesh over the Pacific Ocean domain. **(A)** Pacific ocean domain and **(B)** the focused region (Pacific of Central America) and the mesh spatial resolution.

Central American region boundary and used as initial conditions for the following time steps in the model.

The development of the computational grid must be a trade-off between the spatial resolution and computational cost as an increasing resolution close to the coastline requires a smaller time step in order to ensure stability (explicit methods) or accuracy (implicit methods). Based on this reasoning, a grid with 44,445 computational nodes was established, as shown in Figure 1, which allows the use of high-performance computers to obtain high-fidelity results within feasible computational times. The final mesh resolution ranges from 120 km in the open ocean progressively reducing to 1 km along the shorelines along the Central American Pacific coast.

The numerical model setup involved different tests, taking into account standard model configuration sets for source terms in WWIII. The parametrization families ST4 (Ardhuin et al., 2010; Rascle and Ardhuin, 2013) and ST6 (Rogers et al., 2012; Zieger et al., 2015) provide different sets of physics–mathematical tuning parameters. Both parametrization families mainly consider the effects of wave generation and dissipation, which are adjusted through parameters acting on the governing wave action equation.

The calibration of the model has been carried out by implementing 13 different parametrizations and evaluating both ST4 and ST6 parametrization families. The model parameters were tuned as follows: first, we started with the default values of the parameters proposed in the WWIII manual (WW3DG, 2019); subsequently, we adjusted the values of the parameters related mainly to wind input forcing, atmosphere–sea surface interaction, nearshore bottom friction, and wave energy dissipation through different mechanisms. The aspects mentioned above present parameters or coefficients that have a noticeable influence on the transformation of wave energy density.

These parametrization families allow the WWIII users to calibrate the modeled data to any recorded wave data. Moreover, wind input field databases from ERA-5 (Hersbach et al., 2020), CFSR (Saha et al., 2010), and CFSRv2 (Saha et al., 2014) were employed as forcing conditions. The Unresolved Obstacles Source Term (UOST) WWIII source term package (Mentaschi et al., 2019; 2018; 2015) has been employed to take into account subgrid obstacles, such as small islands. Additional details on the model setup are provided in Table 2.

The WWIII model uses four different time steps to resolve the global, spatial, intra-spectral, and minimum source term time steps, respectively. The evaluated time steps, employed parametrizations, and the wave input data are presented in Tables 3, 4, in which 13 different model parametrizations were evaluated. In particular, ERA5 wind data were used as wind forcing of the WWIII model in 12 of the 13 numerical simulation tests, while the remaining test used the linked databases CFSR and CFSRv2.

The results obtained using the different model setups for the zeroth-order moment wave height (or H_{m0}) have been corrected (i.e., bias adjusted) on the basis of satellite data recollected in the Pacific region of Central America (see Figure 1B). The satellite data have been retrieved from the GlobWave project (Busswell et al., 2010), specifically from the Jason-2, CryoSat, and SARAL satellite missions. The first step involved correcting multiple H_{m0} bins by applying linear regressions between the satellite and modeled H_{m0} values inside each bin, over the increasing ordered distribution of H_{m0}. The number of bins was defined by an iterative process to maximize the correlation coefficient of the linear regressions of each bin while ensuring that each bin contained at least three points. The second step of the H_{m0} correction considered both the wave

TABLE 2 Input data considered in the proposed numerical wave model.

Input information	Source	Spatial resolution	Period	Time resolution
Coastline	SOEST & NOAA Geosciences Laboratory (Wessel and Smith (1996))	50 km (faraway), 10 km (transition), and 1 km (Central American region)	Not applicable	Not applicable
Bathymetry	GEBCO Web Map Service (LLCM, 2020)	15 arc seconds	Not applicable	Not applicable
Wind forcing 1	Wind reanalysis from ERA5 (Hersbach et al., 2020)	Structured grid, 0.30°	1st January 1979 to 31st March 2011	Hourly
Wind forcing 2	CFSRv2 model (Saha et al., 2014)	Structured grid, 0.20°	From 1st March 2011 onward	Hourly

TABLE 3 Configuration of the evaluated ST4 source package. The setup parameter names are in accordance with the nomenclature in the WWIII manual (WW3DG, 2019).

Parameter	Test run ID number									
	1	2	4	7	8	9	10	11	12	13
Δt (s)	Δt_1[a]	Δt_1	Δt_1	Δt_1	Δt_2[b]	Δt_1	Δt_3[c]	Δt_1	Δt_1	Δt_1
ZWND	10.00	10.00	10.00	10.00	10.00	10.00	10.00	10.00	10.00	10.00
ALPHA0	0.0095	0.0095	0.0095	0.0095	0.0095	0.0095	0.0095	0.0095	0.0095	0.0095
BETAMAX	1.60	1.75	1.33	2.00	1.33	1.33	1.33	1.33	1.33	1.60
SINTHP	2.00	1.70	2.00	2.00	2.00	2.00	2.00	2.00	2.00	2.00
ZALP	0.0060	0.0040	0.0060	0.0060	0.0060	0.0060	0.0060	0.0060	0.0060	0.0060
TAUWS.	0.30	−1.00	0.30	0.30	0.30	0.30	0.30	0.30	0.30	0.30
SWELLF	1.00	0.70	1.00	1.00	1.00	1.00	1.00	1.00	1.00	1.00
SWELLF2	−0.018	−0.018	−0.018	−0.018	−0.018	−0.018	−0.018	−0.018	−0.018	−0.018
SWELLF3	0.022	−0.015	0.022	0.022	0.022	0.022	0.022	0.022	0.022	0.022
SWELLF4	1.5E5	1.0E5	1.5E5	1.5E5	1.5E5	1.5E5	1.5E5	1.5E5	1.5E5	1.5E5
SWELLF5	1.20	1.20	1.20	1.20	1.20	1.20	1.20	1.20	1.20	1.20
SWELLF6	0.00	0.00	0.00	0.00	0.00	0.00	0.00	0.00	0.00	0.00
SWELLF7	3.6E5	3.6E5	3.6E5	3.6E5	3.6E5	3.6E5	3.6E5	3.6E5	0.0E1	3.6E5
Z0RAT	0.04	0.04	0.04	0.04	0.04	0.04	0.04	0.04	0.04	0.04
Z0MAX	0.00	0.00	0.00	0.00	0.00	0.00	0.00	0.00	0.00	0.00
SINBR	0.00	0.00	0.00	0.00	0.00	0.00	0.00	0.00	0.00	0.00
GAMMA	−0.067	−0.067	−0.067	−0.067	−0.067	−0.038	−0.038	−0.038	−0.038	−0.067
Wind Input	ERA5	ERA5	ERA5	ERA5	ERA5	ERA5	ERA5	CFSRv2	ERA5	ERA5

[a]Δt_1 [s, s, s, s] = 3600, 1200, 600, 300.
[b]Δt_2 [s, s, s, s] = 900, 900, 600, 300.
[c]Δt_3 [s, s, s, s] = 300, 300, 300, 300.

TABLE 4 Configuration of the evaluated ST6 source package. The setup parameter names are in accordance with the nomenclature in the WWIII manual (WW3DG, 2019).

Parameter	Test run ID number		
	3	5	6
Δt (s)	Δt_1 [a]	Δt_2 [b]	Δt_1
SDSET	T	T	T
SDSA1	0.00000475	0.00000475	0.00000475
SDSP1	4.0	4.0	4.0
SDSA1	0.00007	0.00007	0.00007
SDSP2	4.0	4.0	4.0
SINWS	32.0	32.0	32.0
SINFC	6.0	6.0	6.0
SINA0	0.090	0.040	0.090
CSTB1	F	F	F
SWLB1	0.0041	0.0041	0.0032
CDFAC	1.0	1.0	1.0
C	30,000,000.0	30,000,000.0	30,000,000.0
Wind input	ERA5	ERA5	ERA5

[a]Δt_1 [s, s, s, s] = 3600, 1200, 600, 300.
[b]Δt_2 [s, s, s, s] = 900, 900, 600, 300.

direction of each sea state and the wave energy density distribution in relation to integral parameters belonging to wave spectral partitions, as presented by Albuquerque et al. (2018). The wave-recorded data by satellites and the modeled data are split into wave spectral partitions and wave directions, which were subsequently introduced into a multi-linear regression adjustment. The multi-linear regression between the satellite-recorded and simulated data was performed using Equation 1:

$$H_{sat}^2 = \sum_{i=0}^{15} a_i^2 \, H_{sea,i}^2 + \sum_{i=0}^{15} b_i^2 \, H_{swelli,j}^2 + \epsilon^2 \quad j = 1,2,3, \tag{1}$$

where the subscript i indicates the wave direction bin (width of each bin is 22.5°) and j indicates the number of the three swell partitions provided by the model. The wave spectral energy density is mostly distributed over the sea and the first three swell partitions (De Leo et al., 2024); consequently, these three swell partitions were considered in the H_{m0} correction. If both sea and swell partitions are considered in the correction process, it is called a partitioned correction; instead, if only bulk H_{m0} was considered in the correction expression, it is then called a bulk correction.

Then, several commonly used statistics of fit, such as the Pearson correlation coefficient ρ (see Equation 2), were employed to evaluate the correction procedure:

$$\rho = \frac{\sum_{i=1}^{n} \left(S_i - \overline{S}\right)\left(O_i - \overline{O}\right)}{\sqrt{\left(S_i - \overline{S}\right)^2 \left(O_i - \overline{O}\right)^2}}, \tag{2}$$

where S represents the simulated data and O represents the observations, summed over all i data entries until the total data length n is reached. Likewise, the standard deviation σ and root mean square error $RMSE$ are calculated as shown in Equations 3, 4, respectively:

$$\sigma = \sqrt{\frac{\sum_{i=1}^{n} (\mathrm{err}_i - \mu_{\mathrm{err}})^2}{n}}, \tag{3}$$

where err corresponds to the error between the simulated and observed data and μ_{err} represents the mean value of such errors; the $RMSE$ is defined in Equation 4:

$$RMSE = \sqrt{\frac{1}{n} \sum_{i=1}^{n} (S_i - O_i)^2}. \tag{4}$$

The three statistics mentioned earlier are linked through the so-called Taylor diagram (Taylor, 2001). A water depth criterion has also been evaluated as part of model optimization, which is based on the ratio between the water depth h and the mean wavelength L; then, the model nodes are grouped into deep waters ($h/L \geq 0.05$) and shallow waters ($h/L < 0.05$). Furthermore, the statistical parameter $NSTD$ corresponds to the ratio of the standard deviation of each test's H_{m0} simulated dataset to the standard deviation of H_{m0} of the wave records (reference data). Such standard deviation σ is estimated as presented in Equation 5:

$$\sigma = \frac{\sum_{i=1}^{N} (x_i - \mu)^2}{N}, \tag{5}$$

where x represents each entry in the evaluated database, N is the total number of observations, μ is the mean of the dataset, σ is the standard deviation, σ^2 represents the variance, and ρ corresponds to the Pearson correlation coefficient.

The last stage of the model optimization involved verifying the validity of the wave numerical modeling. Useful wave measurement campaigns from different time windows were gathered from *in situ* wave measurements in the marine regions of El Salvador, Costa Rica, Colombia, and Ecuador, which were compared with the modeled and satellite-based corrected H_{m0}. The details of the wave measurements are listed in Table 5.

Most of the wave records were logged using the acoustic Doppler current profiler (ADCP), as in El Salvador and Costa Rica, and through wave buoys, as in Colombia and Ecuador (see Table 5). The statistics, including ρ, normalized bias NBI, and scatter index SI, were employed to assess the performance of H_{m0} matching in the validation step. The formulas of NBI and SI are shown in Equations 6, 7, respectively:

$$NBI = \frac{\sum_{i=1}^{N} (S_i - O_i)}{\sum_{i=1}^{N} O_i}, \tag{6}$$

$$SI = \sqrt{\frac{\sum_{i=1}^{N} \left(\left(S_i - \overline{S}\right) - \left(O_i - \overline{O}\right)\right)^2}{\sum_{i=1}^{N} O_i}}. \tag{7}$$

TABLE 5 Wave measurements employed in the model validation.

Location	Longitude [°]	Latitude [°]	Period [month/day/year]	Source
Acajutla, El Salvador	−89.86671	13.57202	06/20/2017 to 04/18/2018	MARN, El Salvador (UAIP-MARN, 2021)
Cocos Island, Costa Rica	−87.05545	5.50478	03/01/2018 to 10/15/2018	IMARES, UCR (IMARES-UCR, 2021)
Nicoya Peninsula, Costa Rica	−85.13000	9.55270	01/02/2014 to 04/06/2019	IMARES, UCR (IMARES-UCR, 2021)
$NOAA_{32488}$, Colombia	−77.73700	3.51700	02/13/2019 to 10/16/2009	NOAA (NOAA, 2021)
Salinas, Ecuador	−80.95634	−2.17162	09/05/2013 to 08/18/2014	INOCAR, Ecuador (INOCAR, 2021)

Finally, the parametrization that generated the best adjustment based on the Taylor diagrams described above is then selected and is verified by the model validation. Furthermore, such chosen parametrization was employed to produce the hindcast database employed for the subsequent wave energy resource and WEC assessments.

2.2 Wave energy conversion

Hourly wave data from a period between 1st January 2005 and 30th November 2021 were chosen for the wave energy assessment and WEC performance evaluation. Spectral wave parameters such as H_{m0}, wave peak period T_P, and wavelength L_w were estimated and used for computing the wave power (P_w) through the Equation 8:

$$P_w = \frac{\rho_w \cdot g \cdot H_{m0}^2}{8} \cdot n \cdot \left(1 + \frac{2 \cdot k \cdot h}{\sinh(2 \cdot k \cdot h)}\right) \frac{\omega}{k}, \tag{8}$$

where h is the water depth, ρ_w corresponds to a sea water density of 1,025 $kg \cdot m^{-3}$, g corresponds to the gravitational acceleration (9.81 $m \cdot s^{-2}$), k corresponds to the wave number, and ω is the angular wave frequency. The n term with a value of 1 is employed for intermediate and shallow waters, while n with a value of 0.5 is employed for deep waters (Dean and Dalrymple, 1991). The monthly variation in P_w was determined in the evaluated region, which is estimated by the Equation 9:

$$MV = \frac{\overline{P_{w,hgt}} - \overline{P_{w,lwt}}}{\overline{P_{w,annual}}}, \tag{9}$$

where $\overline{P_{w,lwt}}$ is the month presenting the lowest monthly mean P_w, $\overline{P_{w,hgt}}$ corresponds to the highest monthly mean P_w, and $\overline{P_{w,annual}}$ is the annual average wave power.

Regarding the evaluation of WECs, this study considered the evaluation of one WEC unit per assessed type and not a WEC array. The total energy produced by a WEC, E_0, is estimated, as shown in Equation 10, where $p_{i,j}$ corresponds to the experimental joint frequency of occurrence between H_{m0} and T_e for the total dataset and $PM_{i,j}$ is the power matrix for a specific converter device:

$$E_0 = \frac{1}{100} \cdot \sum_{i=1}^{nT_e} \cdot \sum_{j=1}^{nH_{m0}} p_{i,j} \cdot PM_{i,j}, \tag{10}$$

where T_e corresponds to the wave energy period, i.e., the ratio of the −1 order moment of the wave energy density spectrum over the zeroth-order moment of such a spectrum. The previous E_0 estimation, which is given in Watts per hour, gathers the wave energy that any converter could extract. Additionally, WEC information, such as power matrices for the nine converters, was gathered from several sources: F2HB was obtained from Babarit et al. (2012); Pelamis, SeaPower, Pontoon, AWS, OE Buoy, AquaBuOY, and Langlee features were obtained from Bozzi et al. (2018); and Spar Buoy information was obtained from Rinaldi et al. (2018).

Different indexes expressing the performances of the devices have been employed in order to implement a potential exploitation analysis taking into account several aspects. The capacity factor (CF) represents the theoretical maximum power value, commonly given as a percentage, that the converter can extract over all the hours of 1 year (ΔT), as indicated in Equation 11. The P_0 term, or nominal rated power, corresponds to the maximum power of a given WEC, i.e., the maximum wave energy that can be extracted by the optimal combination of H_{m0} and T_e offered by the WEC power matrix.

$$CF = \frac{E_0}{P_0 \cdot \Delta T} \times 100\%. \tag{11}$$

The assessment of the performance of a WEC using CF does not distinguish between the mean wave regime and extreme wave conditions. Therefore, metrics such as the wave energy development index *WEDI* (Lavidas et al., 2017) and the Selection Index for Wave Energy Deployments $SIWED_{TR}$ (Lavidas, 2020) were designed precisely to depict these kind of matters. In first instance, *WEDI*, calculated by Equation 12, considers the ratio of the annual average wave power over the maximum wave power J_w:

$$WEDI = \frac{\overline{P_w}}{J_w}, \tag{12}$$

where J_w is calculated as the maximum of the P_w series along the time. *WEDI* does not consider the energy conversion devices in it; conversely, $SIWED_{TR}$ considers the CF:

$$SIWED_{TR} = \frac{e^{-CoV_{H_{m0}}} \cdot CF}{\frac{H_{EV\,A}}{H_{max}}}. \tag{13}$$

$SIWED_{TR}$ considers the WEC survivability, given the presence of extreme event evaluation on it (Lavidas, 2020). Indeed, H_{max} in Equation 13 is the maximum wave height, and $H_{EV\,A}$ corresponds to the height obtained from the extreme value analysis (EVA)

methodology, where the EVA considers a probability of occurrence related to a return period (denoted as *TR*) of 30 years. The exponential term in Equation 13 describes the coefficient of variation for H_{m0} (i.e., $CoV_{H_{m0}}$): as wave height variability increases, the $SIWED_{TR}$ decreases, and when the extreme wave height projected for a given device lifetime is less than the maximum value of the significant heights, the $SIWED_{TR}$ value decreases. For the purposes of this study, since a return period of 30 years is considered, the nomenclature of this indicator changes from $SIWED_{TR}$ to $SIWED_{30}$.

The environmental impact of decarbonization (E_{CO_2}) was also estimated by considering the reduction in carbon dioxide emissions when non-renewable sources, in particular natural gas and flared oil, are substituted by wave energy. It is then possible to estimate the amount of avoided tons of carbon dioxide by adopting the relationship presented in Equation 14:

$$E_{CO_2} = \mathrm{EF} \times P_w \times \mathrm{hrs}_{year}, \tag{14}$$

where EF corresponds to the emission factor of 532 g $CO_{2,eq.}/kWh$ for natural gas-fired power plant, whereas an EF factor of 762 g $CO_{2,eq.}/kWh$ is proposed for oil-fired power plant (WG, 2013; Bastos et al., 2023) and P_w considers the potential wave power of each assessed year, produced by an effective converter width of 1 m, over the total number of hours per 1 year, i.e., 8,760 h.

2.3 Scaling of wave energy converters

The energy extraction capacities of the different WECs are modified by the variation in the WEC dimensions. The development of an analysis of possible exploitation depending on the size of the conversion device implies some assumption in the 'scaling' process. Among these assumptions, one of the most important is the use of power matrices for assessing possible WEC energy production. Such WEC power matrices have been resized based on the Froude similarity law. This consideration ensures that the flow regime is indeed turbulent and that the potential energy extracted by the converter being scaled falls within an acceptable range of accuracy (Lin et al., 2024). Additionally, Falcão and Henriques (2014) derived the scaling rules (based on Froude similarity) through dimensional analysis. Sheng et al. (2014) conducted a similar study and concluded that this type of scaling is appropriate but the validity for high Reynolds numbers, an assumption that is taken as true in this evaluation, needs careful consideration. A WEC design must consider not only the production of the power matrix but also the tailored design to be made for specific wave conditions and power production curves, given the respective converter type and mechanical damping characteristics (Cruz et al., 2010). In agreement with previous studies as the one presented by Schmitt and Elsäßer (2017), WECs can scale their geometry but taking into account that power take-off (PTO) scaling is based on device forces and velocities (as opposed to device characteristic length and current velocity for Froude similarity), indicating that the two subsystems do not scale according to the same similarity law.

Adapting the sizes of the WECs allows for more efficient exploitation of the wave climate at a location that could be completely different from the wave climate, for which the specific device has been developed. From a theoretical point of view, this approach requires to adopt a so-called 'similarity'. In the case of sea waves, we employed the *Froude* similarity, equating the *Fr* of the prototype to the *Fr* of the scaled device (Corrales-Gonzalez et al., 2023). Hence, the length scale of the converter is defined as $\lambda = L_m/L_p$, the time is scaled by a factor of $\sqrt{\lambda}$, and the power varies by a factor of $\lambda^{3.5}$ (Windt et al., 2021; Martić et al., 2024). Thus, the captured power by each WEC is scaled based on the aforementioned factor, i.e., all entries of *PM* are multiplied by $\lambda^{3.5}$. Subsequently, the scaled terms E_0 and P_0 produced the scaled CF. The CF-dependent parameters will also be updated with the scaled values. It is worth pointing out that the adjoint occurrence of the wave dataset matrix in the E_0 term, using Equation 10, is not scaled because the wave characteristics over time remain the same and are not affected by the scaling process. Certainly, when a given WEC is scaled, the wave conditions that the WEC interacts with do not necessarily coincide with the highest WEC performance. Therefore, the aim is to precisely adjust the device to its highest efficiency point according to the wave conditions at each studied location. The length reduction scale λ values employed in the present analysis range from 0.2 to 2, with a step of 0.1.

2.4 Sites for wave energy exploitation

The sites for the potential wave energy exploitation analysis were selected based on several aspects, such as their proximity to coastal cities in different countries along the region, the water depth, and the location of the nodes in the mesh of the wave model. The existence of the limit of the continental shelf in the Pacific seaboard has been taken into account in order to limit the costs for installation; the limit has been defined as where the seabed sinks from shallower depths of approximately 300 m to deeper depths of the order of thousands of meters (Lemenkova, 2019). Target locations are shown in Figure 2.

The selected locations for evaluating the wave power exploitation are sited in nearshore regions, and considering that the wave hindcast used was built for a wide domain, the chosen model is well-suited for both applications: WWIII strikes a balance between large-scale oceanic and nearshore wave modeling due to its spectral resolution and capabilities over unstructured grids, allowing for detailed simulations in complex coastal regions. Likewise, WWIII integrates nearshore processes such as refraction, diffraction, and bottom friction with upgraded data processing and handling computational packages.

3 Results and discussion

The present section presents the results obtained during the development of the wave hindcast and discusses the wave exploitation analysis.

3.1 Wave hindcast

The implementation of the hindcast dataset has included the realization of model calibration and tuning at first glance,

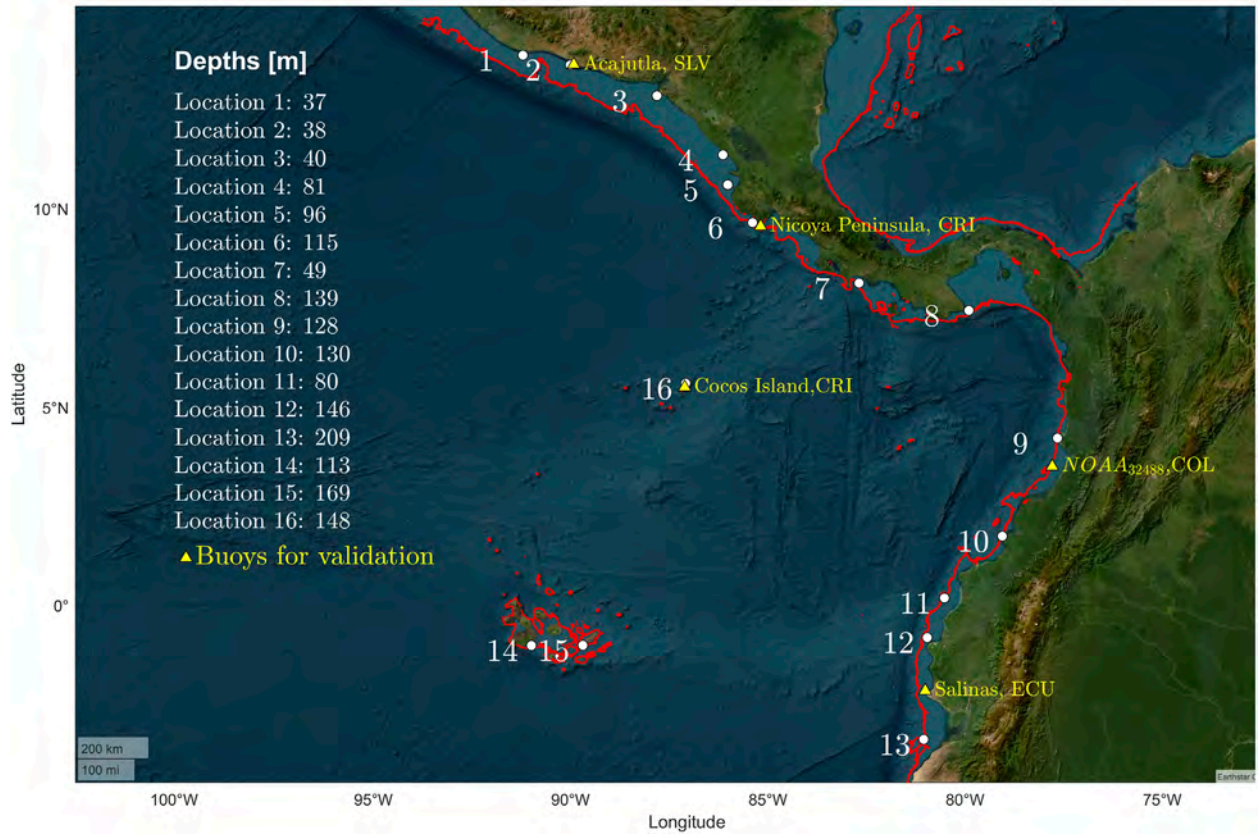

FIGURE 2
Wave energy converter assessment studied sites and locations of the employed buoys in the model validation. Red lines correspond to the 300-m-depth isolines.

employing different settings for the evaluation of the so-called 'source terms' in WWIII; in the second step, the best-performing setting of the model has been compared against the observation in the Pacific coastal zone of Central America using ADCP data for the wave height and wave period. The comparison has been implemented on the bias-adjusted dataset, as illustrated in Section 2.1.

3.1.1 Hindcast calibration

Regarding model test performance, it has been noted that the most promising setting corresponds to the use of the ST4 source terms (setting run test number 10 reported in Table 3). As mentioned in Section 2, the variation in the parameters in the source term packages sought to adjust the coefficients involved in the wave energy transformation processes.

The adjustment between the significant wave height logged by satellite missions and the modeled H_{m0} was further distinguished according to the deep and shallow water criteria. The averaged ρ, σ, and *RMSE*, according to the relations described in Equations 2–4, are shown in Figure 3.

Specifically, it was observed that the test run number 10 matches better with the satellite records for both bulk and partition-based corrections. In the case of the bulk-based correction, *RMSE* values of less than 0.30 m were achieved in most test runs, while for the partition-based correction, the *RMSE* values were greater than 0.30 m and the ρ values are less than 0.7, which leaves out the partitioned correction. Then, it was decided to continue the analysis with the H_{m0} bulk correction.

According to the results presented in rows 2 and 4 of the subplots in Figure 3, it was observed that the bulk correction yielded better fits than the spectral partition-based correction for deep water, shallow water, and all nodes collectively. Additionally, a comparative evaluation with respect to the configurations referred to as *ACC*350 and *T*601 by Ardhuin et al. (2010) was done in this study, identified as run 2 and run 8, respectively. These applied parameterizations did not demonstrate a relevant improvement in the adjustment between the modeled and calibrated H_{m0} and the satellite data.

In terms of water depths at model nodes' locations, the configuration defined in the test run number 10 produces more accurate H_{m0} according to the averaged statistics for all deep water nodes, whereas run 4 produces the best fit for intermediate and shallow waters. According to the H_{m0} correction methodology, there is a not-significant variation between the bulk and partitioned corrections because long period swells approaching from distant southern hemisphere regions (Zheng et al., 2022) are mostly concentrated in a few directional bins, coinciding with the wave directions from which the wind–sea partitions also originate. However, the wave direction discretization into 16 bins, each 22.5°wide, was able to capture more than one bin for the swell events

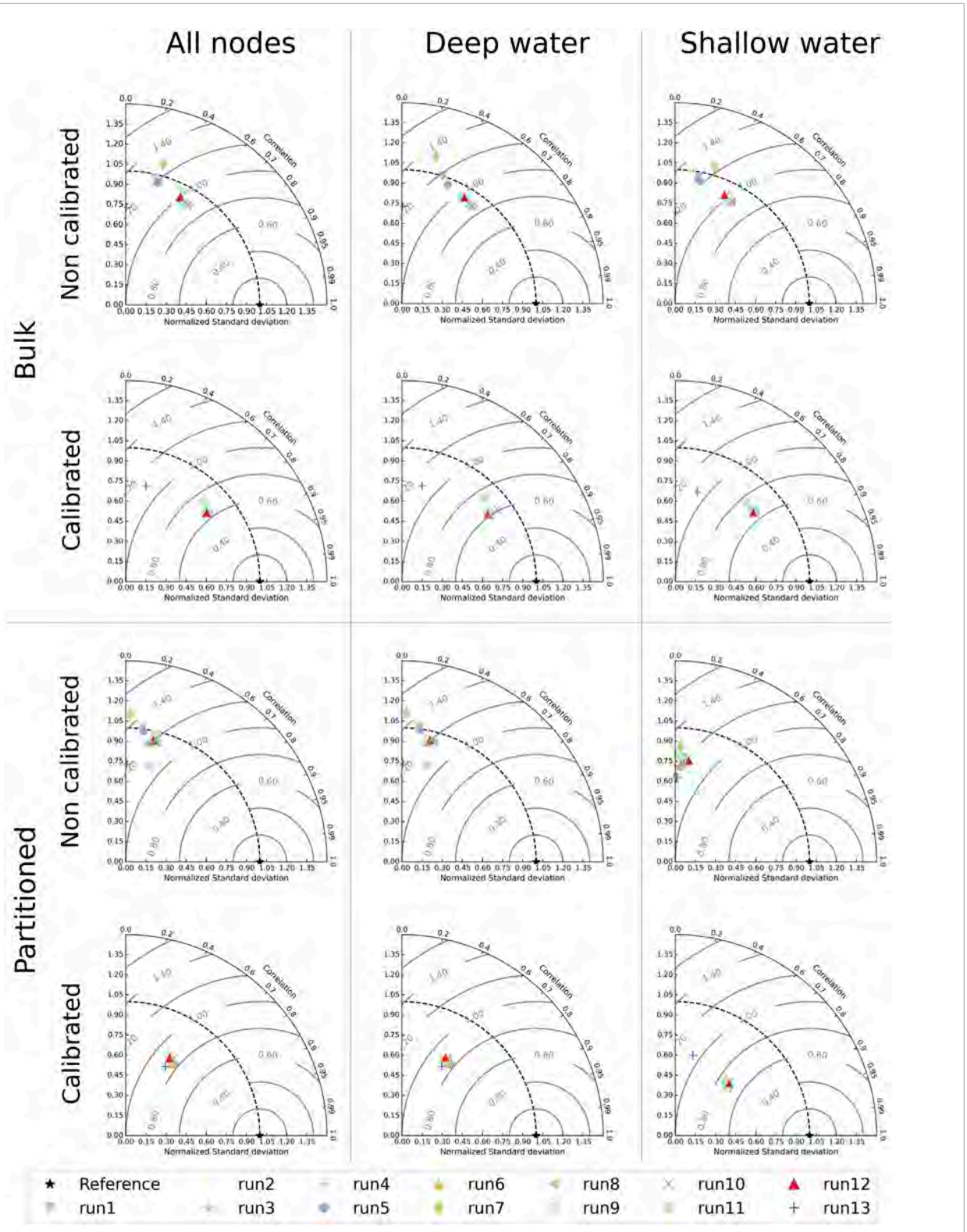

FIGURE 3
Performances of different model setups without calibration and with calibration (bulk and partitioned) for different sets of grid nodes depending on the water depth.

and more than three bins in cases where wind–wave local events dominated. The setup of the model chosen for the development of the study corresponds to the test run 10.

The turbulent Reynolds numbers present in the ST4 source term package were also evaluated by varying the swell parameter dissipation processes (Re_c, according to the WWIII manual

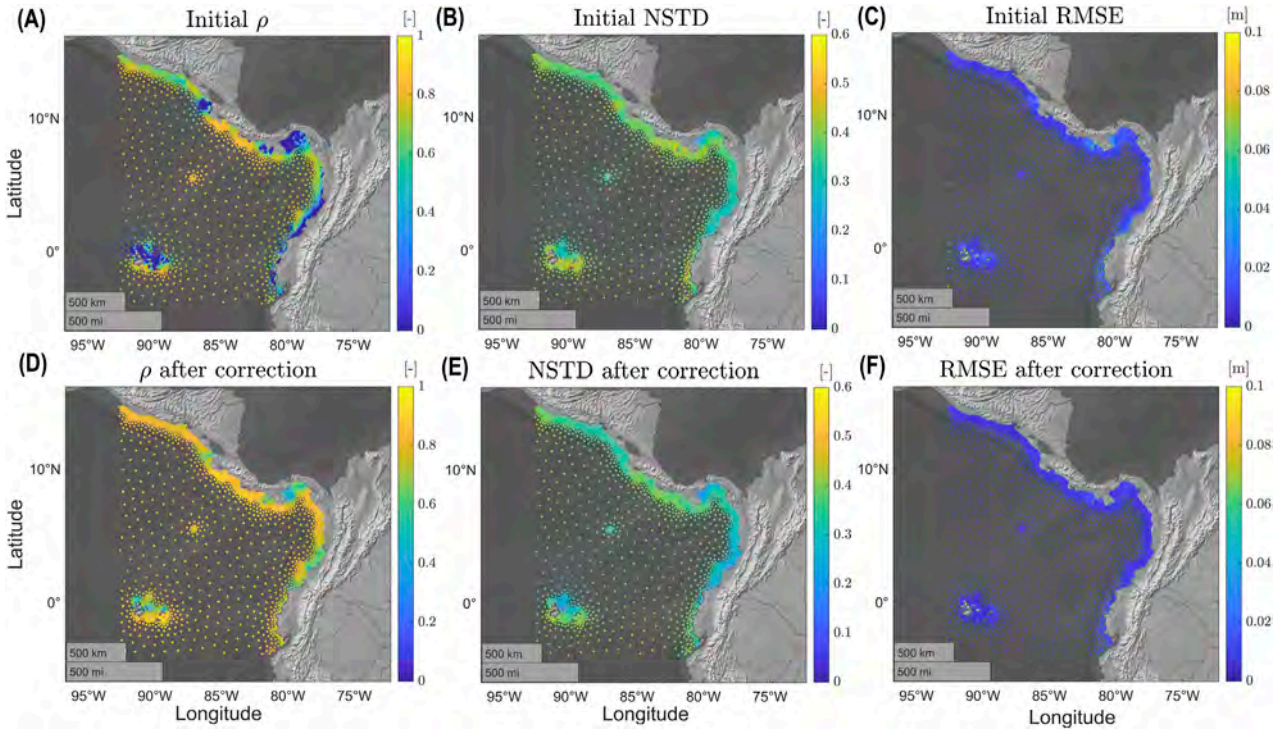

FIGURE 4
Goodness-of-fit statistics at the computational nodes by employing the optimized model (test run 10, bulk correction): **(A)** ρ before correction, **(B)** σ before correction, **(C)** *RMSE* before correction, **(D)** ρ after correction, **(E)** *NSTD* after correction, and **(F)** *RMSE* after correction.

(WW3DG, 2019)). However, this evaluation does not substantially increase the accuracy, according to the results shown in Figure 3.

This choice is based on the fact that although the test runs 9 and 10 are the best-performing setups, test run 10 presents a more efficient correction based on bulk parameters rather than test run 9, which requires the partitioned correction.

Figure 4 reports a summary of the performances for the chosen set-up of the model (run 10 considering bulk correction) before and after the bulk correction. The values of the error indicators reveal that the model performs better in deep waters than in shallow waters (as already depicted in Figure 3).

It was noted that the correlation tends to be lower in deep water rather than in the coastal regions, as shown by the statistics in panels (D), (E), and (F) of Figure 4. Run 10 produced the highest ρ of 0.7729 for all nodes, and ρ equals to 0.7971 for the deep water nodes. Likewise, run 10 produces the highest ρ value of 0.7556 for the shallow waters nodes. Additionally, a lower accuracy in the adjustments is noted in the northeast region of the Galapagos Islands and shallow waters regions such as the Southern nearshore region of Nicaragua, the Gulf of Chiriqui, and the Gulf of Panama, as well as the Southern nearshore region of Colombia. Improvements in the adjustments were achieved with the bulk correction of the deep water nodes (Figure 4E), compared to the shallow water nodes or all nodes together; however, the absolute difference in *RMSE* between the fit of run 10, as shown in Figures 4D, E, is 0.06 m. Run 10 produced the highest mean ρ of 0.7729 by considering all nodes, while a mean ρ of 0.7971 was achieved when deep water nodes were considered in such an averaged value. Concerning the spatial adjustments, charts (A) and (D) of Figure 4 show that the mean ρ values increased particularly in nearshore regions, increasing from mean values of less than 0.2 to new values greater than 0.6 in many regions. Specifically, in the nearshore region of the Gulf of Panama, the mean ρ values do not exceed 0.6 even if the error statistics improved substantially with respect to the values prior to the correction. Deep water nodes have improved their spatial goodness-of-fit statistics, with mean ρ values increasing from 0.80 to over 0.90 (see Figure 4).

3.1.2 Model validation

Once the H_{m0} correction has been developed based on satellite data, the validation of the model reliability has been performed against *in -situ* wave measurements, as mentioned in Section 2.1 and detailed in Table 5. Field observations were available at five specific locations for different time windows and have been employed to compare the modeled wave integral quantities against the observed ones. Among the five locations, only two have continuous recordings (Acajutla and Salinas), while the other three had some gaps due to interruptions in the monitoring activities (maintenance and breakdowns). Figure 5 presents the comparison of the calibrated modeled data and the wave measurements using scatter plots for integral quantities: H_{m0}, T_p, and D_p. The results show that modeled H_{m0} data approximate the measured records with higher precision in the medium regime than in extreme regimes. Indeed, Nicoya and Salinas locations have shown the largest H_{m0} underestimation bias. Statistics demonstrated the acceptable

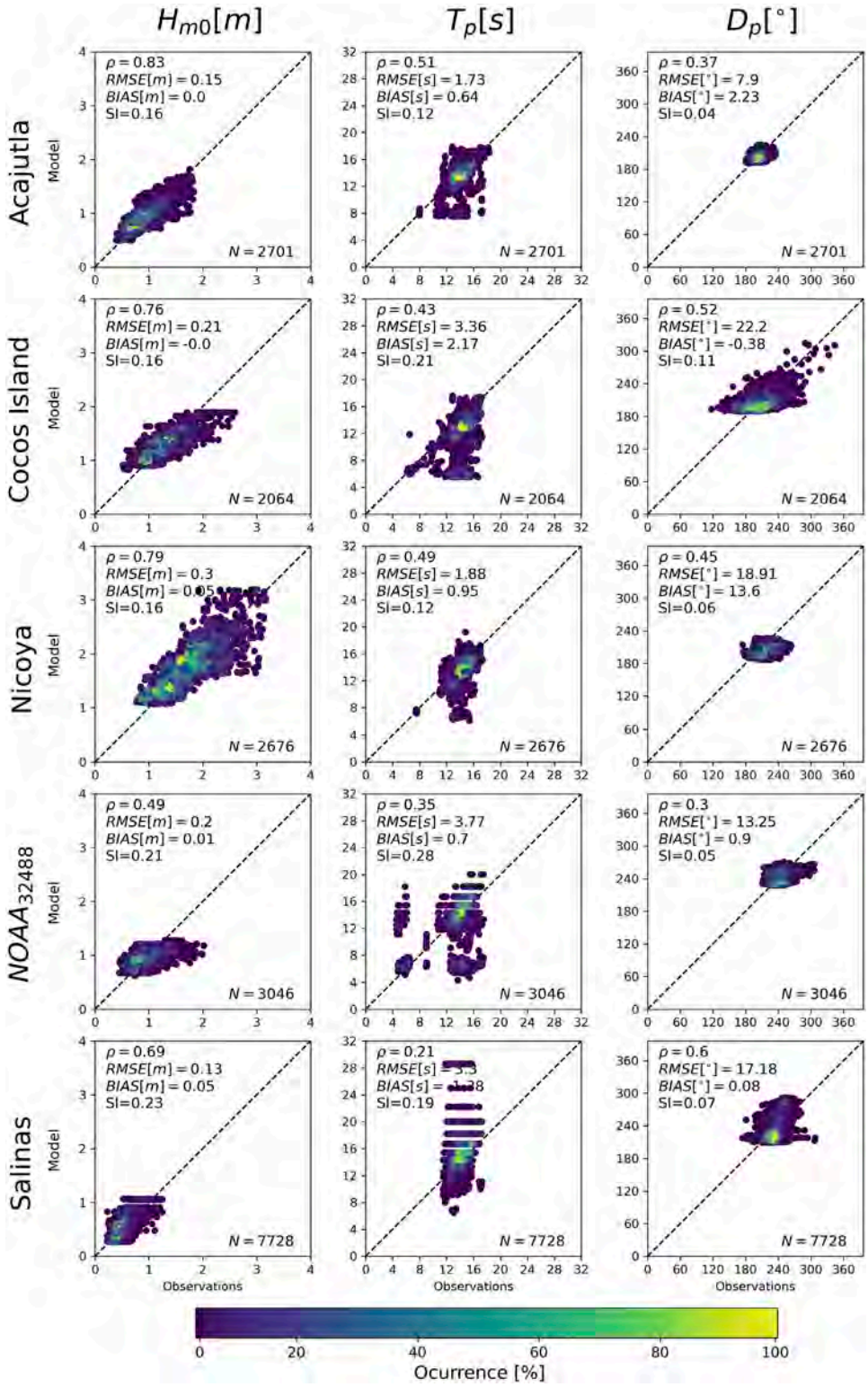

FIGURE 5
Model vs. observation frequency for H_{m0} (left column), T_p (central column), and D_p (right column). The N value in the lower right corner of the graphs indicates the number of samples considered.

agreement for H_{m0} at the evaluated locations, providing ρ values above 0.70 for most of the locations, except the value of 0.49 in $NOAA_{32488}$. In case of T_p, more dispersion appeared over the whole range of the data with respect to H_{m0}. WWIII computes T_p based on a wave spectrum function that discretizes it into period bins selected during the model setup. Lower values of ρ

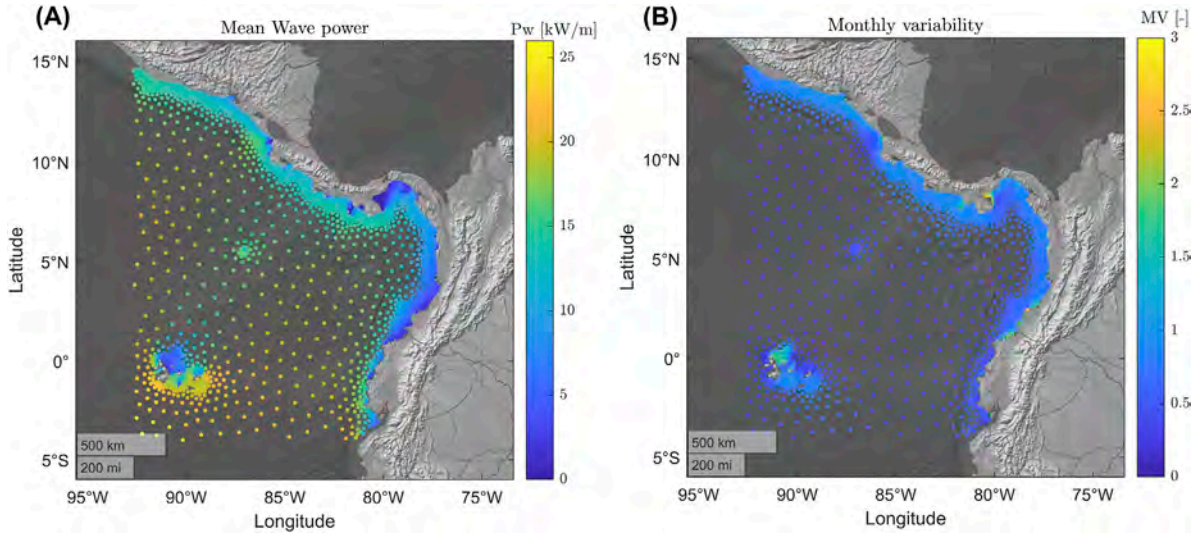

FIGURE 6
Annual mean wave power **(A)** and monthly variability *MV* **(B)**.

were observed for periods with respect to H_{m0}, with the highest value of this parameter (0.51) recorded at the Acajutla location. More dispersed scatter points, i.e., those lying farther from the diagonal bisector, were observed at Cocos Island, $NOAA_{32488}$, and Salinas than at the rest of the locations. It was observed that the coastal location Salinas presented the highest mismatch of T_p, with some observations between 12 and 16 s being overestimated by the model, reaching values over 20 s. Regarding D_p, ρ correlations lower than 0.6 appeared over all the validation locations. However, low dispersion occurred based on the *SI* indexes. Most of the validation locations are located in the nearshore of the American continent, except for the Cocos Island, where there is more variability in the wave direction observations. However, the predominant wave direction over the Pacific of Central America (south–southwest) is acceptably estimated, yielding scatter points surrounding the diagonal bisector in the plots in column 3 of Figure 5. In this case, the worst adjustment was found at the Cocos island buoy, where the *RMSE* value is 22.20° wherein high wave directional spreading occurs. Furthermore, the lowest *RMSE* was found in Acajutla with a value of 7.90°. *RMSE* values between 13.2° and 18.9° were found in the rest of the locations. In summary, comparisons between the observations and the model showed that the scattered point cloud is concentrated along the diagonal bisector (indicating perfect correlation); however, such scattered points tend to lose accuracy depending on the validation location.

3.2 Wave energy exploitation

3.2.1 Wave energy assessment

A preliminary insight into the availability of the wave energy resource can be derived from the spatial distribution of the wave energy flux across all grid points in the numerical domain for the Central American Pacific zone.

Figure 6 presents the mean annual P_w and its monthly variability. Notable spatial variability in P_w was observed over the studied region, with deep water locations showing the mean and maximum values of 21.7 and 25.1 kW/m, respectively. In nearshore regions, mean values range from 4.3 to 11.4 kW/m. The above-mentioned magnitudes classify this region as having a medium energy potential at a global level (Foteinis, 2022). However, these values vary in time and are influenced mainly by the metocean events occurring at large scales in the Pacific Ocean, as well as the regional and local storms. Regarding the seasonality, it is worth noting that in inter-tropical regions, there is no clear distinction between the months presenting high extreme events/low energy periods and their maximum/minimum peak values, unlike the clear seasonality identified at higher latitudes. The regions exhibiting the highest variability in seasonal and monthly metrics (SV and MV, respectively) include the shallow waters near the Galapagos Islands, the area adjacent to the southern coast of Colombia, the eastern Gulf of Panama, and the vicinity of the Gulf of Fonseca in southern Honduras, with values ranging between 1.5 and 2. Previous research in the Pacific Ocean has identified seasonal influences such as low atmospheric pressure systems, polar wind fronts from mid-latitudes, and oceanic currents, some of which have caused natural disasters in the region (Zhao et al., 2020; Portilla-Yandún et al., 2020). These studies suggest patterns in wave energy behavior over time. However, these patterns are not consistent across the Pacific of Central America, where regional or local atmospheric events also play a significant role. Although the total energy potential of ocean waves is impossible to extract, the computed wave power data allow us to corroborate the potential energy content in the region and also provide a spatial and temporal description of the variation in wave energy potential.

3.2.2 Performance of wave energy converters

A preliminary analysis of WEC performances has been implemented on the basis of different indices commonly employed

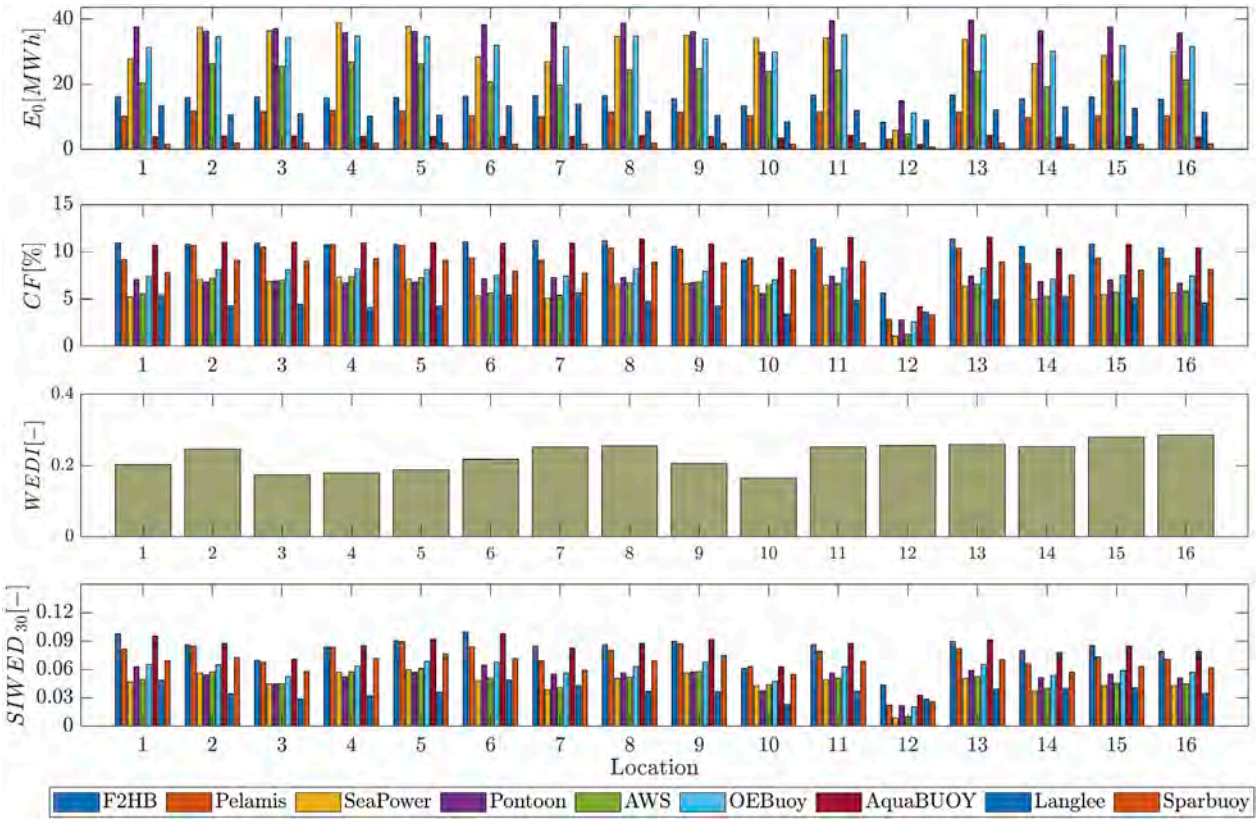

FIGURE 7
WEC performance indexes: E_0, device potential energy production; CF, capacity factor; *WEDI*, wave energy deployment index; and $SIWED_{30}$, selection index for wave energy development.

in the literature for this type of assessment. Figure 7 shows the main findings of the wave energy assessment analysis and the potential exploitation of the energy potential. In particular, the potential energy production E_0 for the different devices at different locations is shown in the top panel. The results suggest that, for a single device, the most productive options are Pontoon, SeaPower, OE Buoy, and AWS. It should be noted that some devices (like the point absorbers) could produce low output for a single device but are usually installed in arrays; in other words, the effective production of a device farm could be significant even if the nominal production of a single device is small.

At first glance, the results clearly show that for all the indexes taken into account, location 12 is not promising at all for a possible wave energy exploitation project because it presents low values of E_0, CF, and $SIWED_{30}$. The results also show that WEC units SeaPower, Pontoon, and OE Buoy are able to produce more than 30 MWh at almost all the locations (except for location 12).

In order to understand the potentiality of possible wave energy harvesting in the target area, we can refer to socio-economic statistics of the region (WorldBank, 2014), which indicate that the electricity consumption *per capita*, in the area between Guatemala and Ecuador (i.e., Central America region), ranges between values of approximately 500 and 2,100 kWh. Thus, even if wave energy exploitation cannot completely substitute non-renewable energy source of the coastal area of the region, it could anyway represent a valid ingredient of the energy mix for the countries of the Central America region if properly optimized and designed.

We explored the information provided by *WEDI* and $SIWED_{30}$ indexes, as reported in the respective panels of Figure 7. These indexes take into account the frequency and intensity of extreme events. *WEDI* does not consider the specific WEC deployment, relying just on the variability of the wave energy between the extreme values and the average regime. On the other hand, $SIWED_{30}$ takes into account the extreme events over a time horizon that is usually defined by the operator on the basis of possible extension of the lifetime of the wave energy exploitation project. This approach allows to take into account the survivability and operability of the WECs.

In addition, CF does not provide an overall view of the amount of energy supplied during a given period, but it just provides the 'efficiency' of the selected WEC, while E_0 gives an estimate of the maximum possible energy exploitation that can be attained in a specific location. For the evaluation of E_0, we considered a 'cut-off' mechanism for the devices in order to take into account the downtime periods when metocean conditions exceed operational conditions for the different WECs (i.e., values of H_s and T_p fall out of the range provided by the *PM*).

Moreover, the inefficiency of the *WEDI* term to evaluate converters and its inability to compare with $SIWED_{30}$ is highlighted. For example, discrepancies of such parameters between F2HB and

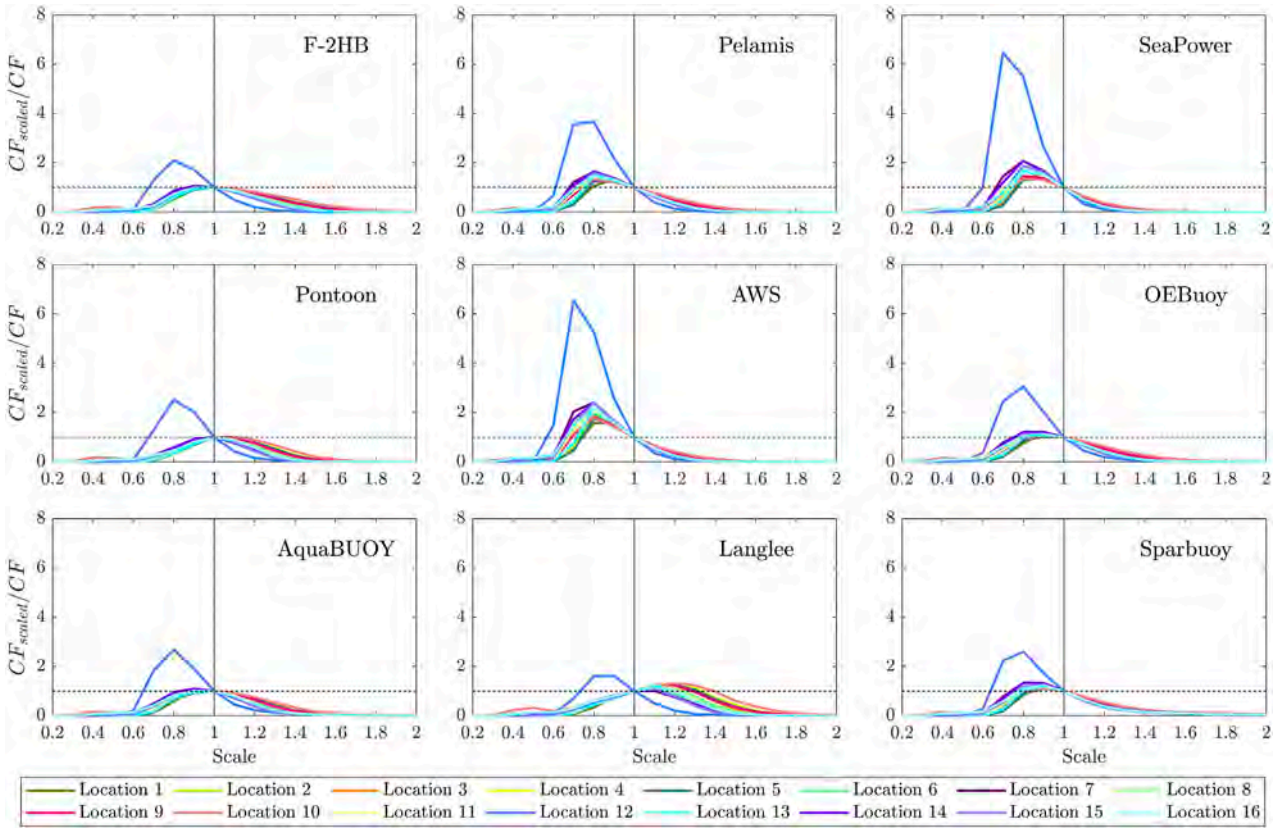

FIGURE 8
CF ratios of the scaled WECs over the prototype ones (λ = 1) at the studied sites.

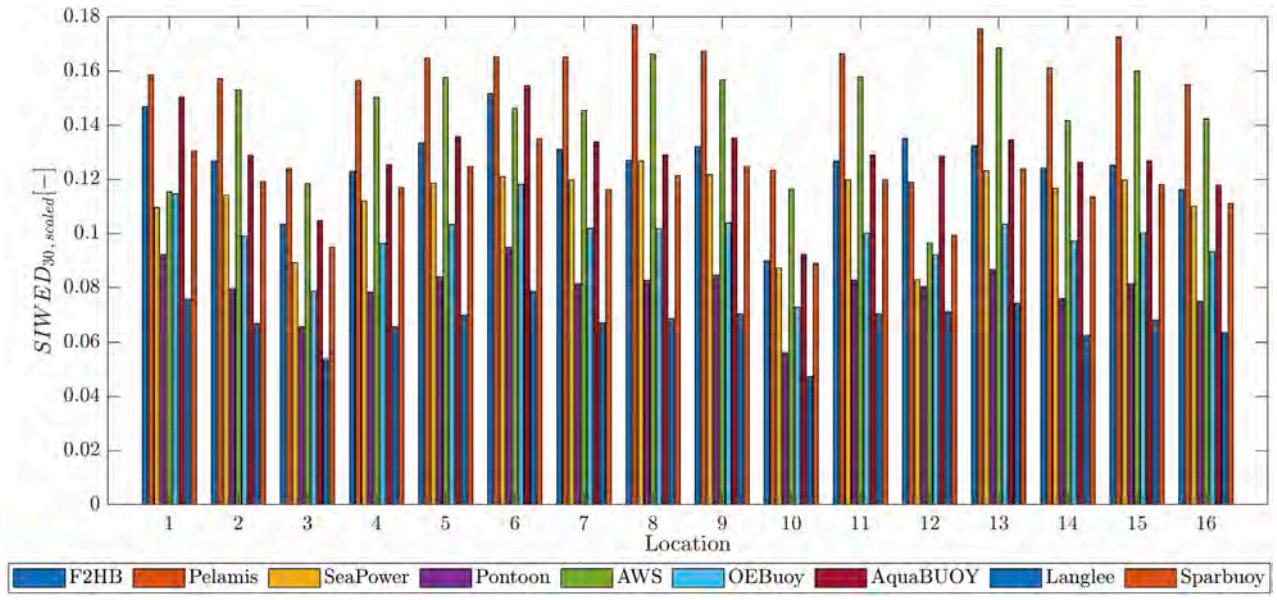

FIGURE 9
$SIWED_{30}$ for scaled WECs with λ maximizing the capacity factor CF.

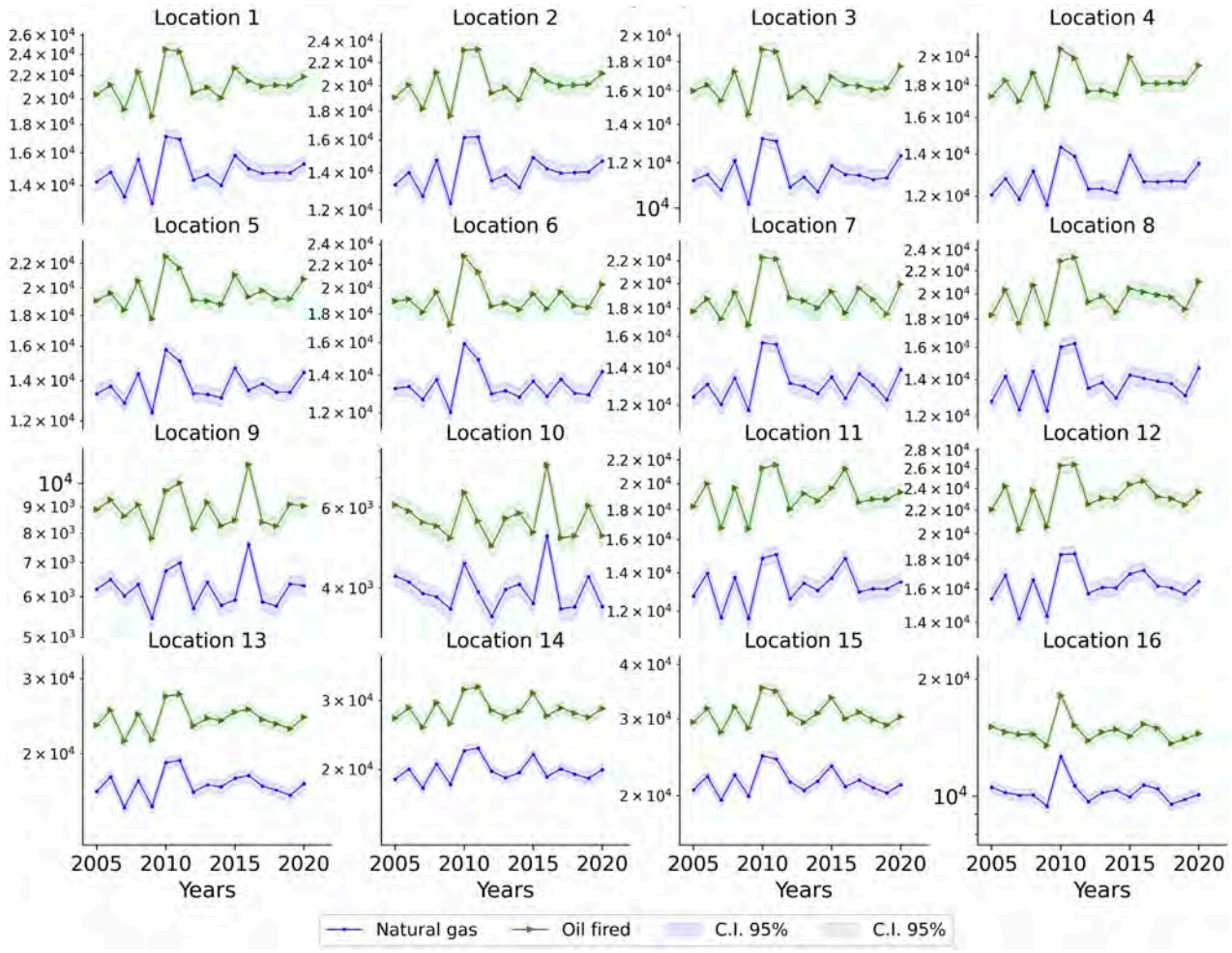

FIGURE 10
Avoided CO_2 emissions by substituting fossil fuel energy sources with wave energy at the studied sites. Vertical axes indicate tons.

AquaBuOY were found for the same location. Both converters offer the highest $SIWED_{30}$ among all WECs at location 1, and both correspond to the most feasible options at this location, whereas *WEDI* makes no distinction between converters. This fact implicitly indicates which converters are less vulnerable to downtime due to storm events.

A further evaluation was conducted seeking a higher performance on the WEC extraction, such as through WEC scaling. Figure 8 presents the amount of increase in the capacity factor with respect to the prototype value for the 9 assessed converters at all 16 locations. It is interesting to note that location 12 is the most affected in terms of CF by the optimization of the device scale, with the scaled CF increasing up to more than six times when the AWS converter is employed. Still, in the case of location 12, WEC downsizing produced a CF competitive with others achieved in other locations, as shown in the CF trends in Figure 7.

An interesting finding is related to the Langlee converter: unlike the other WECs, Langlee requires an upsizing of its dimensions to improve the CF, with scales λ varying between 1.1 and 1.2. Then, its CF is increased by up to about 30%. Pelamis, SeaPower, and AWS converters would be the most feasible scaled WECs from the technical point of view along this region. In particular, the AWS converter is positively impacted by scaling it down, reaching more than 56% of its CF for all locations and even reaching 6.54 time more than the prototype CF at location 12, if the device is scaled at a λ value equal to 0.7.

SeaPower reaches similar values as the previous one, an increase of 35% in the CF at all locations, and the highest CF corresponds to 6.45 times more than the CF prototype at location 12. The distinct behavior in location 12 based on the performance indexes, i.e., the lowest $SIWED_{30}$ and *WEDI* among the all locations, is due to specific morphology of that location being in the shadow region produced by the De la Plata island: wave energy potential is, hence, limited by the specific interaction between the incoming waves and the presence of obstacles and the specific bathymetry.

Finally, the WEC-producing higher CF corresponds to the AWS when scaled with a λ value equal to 0.7 at location 12 and a λ value equal to 0.8 from locations 1 to 11 and from 13 to 16. However, because the classification of the best option for the choice of a possible wave energy converter in a specific location also depends on the economic assessment, an evaluation of just the capacity factor it is not enough and not exhaustive for the

development of an exploitation project (Guo et al., 2023; Vanegas-Cantarero et al., 2022).

The scaling procedure allowed us to estimate new results for the *SIWED* index. We developed the evaluation of *SIWED* at all the locations for all the devices, taking into account the value of λ that maximizes the value of the CF in order to have an insight into the effect of scaling on the *SIWED*. Figure 9 presents the resulting $SIWED_{30}$ when WEC scaling was done. Pelamis was the most benefited converter from the scaling for all the sites studied although the AWS also increased its efficiency. The Pelamis converter's harvesting capabilities depend on its longitudinal placement parallel to the predominant wave direction, implying that energy production is closely related to the typical wave periods, which, in the case of the evaluated region, based on the results obtained, prove to be beneficial for this type of converter.

It was evident that for all converters, the SIWED magnitudes were significantly increased when scaling is performed. The Langlee converter, whose CF was increased by upsizing the WEC in the majority of locations (see Figure 8), significantly increased the magnitude of $SIWED_{30}$; however, such WECs are found to be the least efficient among the rest at all the sites.

Finally, we also analyzed the possible impacts on the environmental side, developing a preliminary estimation of the savings in fossil fuel consumption for energy production if wave energy exploitation were to be developed in the Pacific coastal zone of Central America. Based on the average values for all locations shown in Figure 10, approximately up to 3,977.0 tons of CO_2 by substituting natural gas or approximately 5,696.4 tons of CO_2 potentially produced by oil-fired combustion, could be avoided if these combustible energy sources are replaced by wave energy.

Location 9 corresponds to the place where the equivalent avoided CO_2 would be the highest along the region, with annual average values of 8,964.5 tons of CO_2 (by substituting oil fired) and 6,303.7 tons of CO_2 (by substituting natural gas). When comparing these values with the average annual CO_2 emissions of Nicaragua, the lowest CO_2 emitter in 2020 in the studied region (WorldBank, 2023, 4,582,000.00 tons of CO_2), we can state that the actual figures should be analyzed in a more detailed way through specific wave exploitation projects in order to obtain more accurate estimates and aim for a reasonable percentage reduction in $C0_2$ emissions for energy production.

Nevertheless, no legal framework was established regarding the WEC implementation along the studied region, given the lag in the issue of marine energy deployment, thus hindering a proper socio-economic assessment of wave energy converters. Thus, it makes it difficult to define the optimal number of WECs needed in a farm to meet a specific electrical energy demand, whether using prototypes or scaled up versions. Nowadays, there are policies such as guidelines dictated by the International Organization for Standardization (ISO) guidelines for the life cycle assessment of converters (Zhai et al., 2021) that can be adopted and adapted to this region.

Furthermore, the marine ecological agreement between countries in this region could be taken as a starting point for the discussion and delimitation of marine energy exploitation areas. Although in recent years, first investigations on marine energy conversion were encouraged through conferences and incentives for countries in this part of the world (Shadman et al., 2023), there is still a long way to go. Further exploration on the subject will definitely contribute to achieving sustainable development goals and advancing the use of clean energy in the coming years.

4 Conclusion

The first part of this study describes the generation of a new wave hindcast, its optimization, and its validation over the Central American Pacific region with high spatial and time resolution from 1980 to 2021. Then, several tests of the WWIII model configuration have been assessed, including the evaluation of two source terms packages. It is concluded that the ST4 terms package (Ardhuin et al., 2010; Rascle and Ardhuin, 2013) provides the best model performance compared to satellite data for H_{m0} using ERA5 wind forcing (Hersbach et al., 2020).

In addition, bias adjustment for the wave significant height has been implemented using a two-step H_{m0} correction process, i.e., a bias adjustment followed by the multi-linear regression of H_{m0} (Albuquerque et al., 2018). Once the hindcast has been calibrated and optimized using the two-step bias adjustment approach, its reliability has been assessed through validation against field measurements located in the coastal region of Pacific Central America. The findings allowed us to identify the best setup of the model, as shown in Table 3, that has been employed for the wave energy potential exploitation assessment.

The validated hindcast database can be used for various ocean and coastal applications such as the design of structures and/or for climatic and wave analysis due to its high resolution in space and time (hourly resolution for the entire period). The hindcast comprises integral quantities (H_{m0}, T_p, T_{02}, and T_{m01}) and quantities of spectral partitions related to wind waves and three swell components. Furthermore, wind components at 10-m height are provided over the nodes of the unstructured grid of a high spatial resolution. This alleviates one of the limitations of many atmospheric models, such as a low spatial resolution for coastal applications, providing more reliable and accurate wind data to feed the wave model. However, there may be local wind events that the low resolution of global atmospheric numerical models fails to capture and would lead to additional validation of the downscaled wind data, which is not part of the present study.

The results of the wave energy assessment suggested that the Pacific region of Central America presents a medium wave energy potential with respect to global wave energy potential. However, the wave energy exploitation could be promising due to the low variable wave conditions throughout the year, as shown by the monthly variability analysis. In addition, resizing and adapting the energy converters to the average wave conditions in such a region can lead to an increase in the performances of the exploitation through significant increases of the target indexes employed in the study (CF, *WEDI*, and *SIWED*). The assumptions considered for the WEC scaling conditioned the validation of the similarities between the scaled model and the prototype in terms of the interaction of wave action and device, which are beyond the scope of this study.

In terms of WEC performance assessment, the feasibility of the

$SIWED_{30}$ indicator is verified to define the technical performance of the deployment of wave converter at any world latitude combining all resource, power production, and extreme information into an unbiased approach. By doing so, it is possible to compare the energy extraction from waves by various converters if they are installed in locations with different wave climate characteristics (different regions of the world, for example).

In conclusion, the best converter, in terms of WEC efficiency over time, for all locations corresponds to Pelamis, based on the *WEDI* and $SIWED_{30}$ indexes, although the F2HB converter also presented a significant efficiency, both at reduced scales. The presence of swells reaching the Central American Pacific region turned out to be favorable for converters such as Pelamis, whose energy transformation mechanism works because its placement is related to the direction of wave propagation and its wavelengths. The WEC evaluation using indexes returns some key insights: the performance indexes of converters should take into account economic evaluations of the affordability of the possible exploitation projects, both in terms of capital expenditures and operational expenditure for the lifetime of the devices.

It was demonstrated that the abandoning non-renewable energies produced from natural gas and oil (fossil fuels) contributes to the achievement of the goal 7 of the 2030 Agenda, which focuses on universal access to affordable, reliable, and modern sustainable energy for all.

The present study achieves the two fundamental research objectives: first, the development of optimized wave hindcasting data over the Pacific Ocean with high space and time resolution in the Central American zone and, second, the evaluation of potential wave energy exploitation using technical indexes, representing a pioneering evaluation throughout the assessed region.

Data availability statement

The raw data supporting the conclusions of this article will be made available by the authors, without undue reservation.

Author contributions

MC-G: data curation, investigation, methodology, project administration, visualization, writing–original draft, writing–review and editing. GL: conceptualization, formal analysis, methodology, writing–original draft. AL-L: conceptualization, supervision, writing–original draft. GB: conceptualization, funding acquisition, supervision, writing–original draft, writing–review and editing.

Funding

The author(s) declare that no financial support was received for the research, authorship, and/or publication of this article.

Acknowledgments

MC-G would like to express gratitude to the Ocean Energy Systems and their research scholarships, OES-BECS, and the International Network on Offshore Renewable Energy (INORE) for partially supporting this study through an award in 2022. CINECA is acknowledged for providing computational resources under the ISCRA-C projects: WPAC-1, WPAC-2 and WPAC-3. The authors also acknowledge the Oceanographic Institute of the Navy INOCAR of Ecuador, the Marine, River, and Estuarine Engineering Unit IMARES of the University of Costa Rica and the Ministry of Environment and Natural Resources MARN of El Salvador for providing the wave data required for the validation of the wave model.

Conflict of interest

The authors declare that the research was conducted in the absence of any commercial or financial relationships that could be construed as a potential conflict of interest.

Publisher's note

References

Aderinto, T., and Li, H. (2019). Review on power performance and efficiency of wave energy converters. *Energies* 12, 4329. doi:10.3390/en12224329

Albuquerque, J., Antolínez, J. A., Rueda, A., Méndez, F. J., and Coco, G. (2018). Directional correction of modeled sea and swell wave heights using satellite altimeter data. *Ocean. Model.* 131, 103–114. doi:10.1016/j.ocemod.2018.09.001

Amarouche, K., Akpınar, A., Bachari, N. E. I., and Houma, F. (2020). Wave energy resource assessment along the algerian coast based on 39-year wave hindcast. *Renew. Energy* 153, 840–860. doi:10.1016/j.renene.2020.02.040

Amrutha, M., and Kumar, V. S. (2019). Changes in wave energy in the shelf seas of India during the last 40 years based on era5 reanalysis data. *Energies* 13, 115. doi:10.3390/en13010115

Ardhuin, F., Rogers, E., Babanin, A. V., Filipot, J.-F., Magne, R., Roland, A., et al. (2010). Semiempirical dissipation source functions for ocean waves. part i: definition, calibration, and validation. *J. Phys. Oceanogr.* 40, 1917–1941. doi:10.1175/2010jpo4324.1

Arinaga, R. A., and Cheung, K. F. (2012). Atlas of global wave energy from 10 years of reanalysis and hindcast data. *Renew. Energy* 39, 49–64. doi:10.1016/j.renene.2011.06.039

Babarit, A., Hals, J., Muliawan, M. J., Kurniawan, A., Moan, T., and Krokstad, J. (2012). Numerical benchmarking study of a selection of wave energy converters. *Renew. energy* 41, 44–63. doi:10.1016/j.renene.2011.10.002

Bastos, A. S., Souza, T. R. C. d., Ribeiro, D. S., Melo, M. d. L. N. M., and Martinez, C. B. (2023). Wave energy generation in Brazil: a georeferenced oscillating water column inventory. *Energies* 16, 3409. doi:10.3390/en16083409

Beyá, J., Álvarez, M., Gallardo, A., Hidalgo, H., and Winckler, P. (2017). Generation and validation of the chilean wave atlas database. *Ocean. Model.* 116, 16–32. doi:10.1016/j.ocemod.2017.06.004

Björkqvist, J.-V., Vähä-Piikkiö, O., Alari, V., Kuznetsova, A., and Tuomi, L. (2020). Wam, swan and wavewatch iii in the Finnish archipelago–the effect of spectral performance on bulk wave parameters. *J. Operational Oceanogr.* 13, 55–70. doi:10.1080/1755876X.2019.1633236

Boungou, W., and Yatié, A. (2022). The impact of the Ukraine–russia war on world stock market returns. *Econ. Lett.* 215, 110516. doi:10.1016/j.econlet.2022.110516

Bozzi, S., Archetti, R., and Passoni, G. (2014). Wave electricity production in Italian offshore: a preliminary investigation. *Renew. Energy* 62, 407–416. doi:10.1016/j.renene.2013.07.030

Bozzi, S., Besio, G., and Passoni, G. (2018). Wave power technologies for the mediterranean offshore: scaling and performance analysis. *Coast. Eng.* 136, 130–146. doi:10.1016/j.coastaleng.2018.03.001

Busswell, G., Ash, E., Piolle, J.-F., Poulter, D., Snaith, H., Collard, F., et al. (2010). "Project globwave," in *Proceedings of the third international workshop SeaSAR 2010, held at ESA ESRIN (frascati, Italy)*, 25–29. January, 2010).

Center, N. (2006). *2-minute gridded global relief data (etopo2) v2*. United States: National Geophysical Data Center N.

Chawla, A., Tolman, H. L., Hanson, J. L., Devaliere, E.-M., and Gerald, V. M. (2009). Validation of a multi-grid wavewatch iii modeling system. *NOAA/MMAB Contrib.*, 281.

Contestabile, P., Ferrante, V., and Diego, V. (2015). Wave energy resource along the coast of santa catarina (Brazil). *Energies* 8-12, 14219–14243. doi:10.3390/en81212423

Cornett, A. M. (2008). "A global wave energy resource assessment," in *ISOPE international Ocean and polar engineering conference (ISOPE)* (Ottawa, Canada: ISOPE–I).

Corrales-Gonzalez, M., Lavidas, G., and Besio, G. (2023). Feasibility of wave energy harvesting in the ligurian sea, Italy. *Sustainability* 15, 9113. doi:10.3390/su15119113

Cruz, J., Sykes, R., Siddorn, P., and Taylor, R. E. (2010). Estimating the loads and energy yield of arrays of wave energy converters under realistic seas. *IET Renew. Power Gener.* 4, 488–497. doi:10.1049/iet-rpg.2009.0174

CMEMS (2021). Global ocean waves reanalysis waverys. doi:10.48670/moi-00022

Dean, R. G., and Dalrymple, R. A. (1991). *Water wave mechanics for engineers and scientists*, 2. Singapore: world scientific publishing company.

Decastro, M., Rusu, L., Arguilé-Pérez, B., Ribeiro, A., Costoya, X., Carvalho, D., et al. (2024). Different approaches to analyze the impact of future climate change on the exploitation of wave energy. *Renew. Energy* 220, 119569. doi:10.1016/j.renene.2023.119569

De Leo, F., Cremonini, G., Corrales-González, M., and Besio, G. (2024). Climate analysis of wave systems for multimodal sea states in the mediterranean sea. *Appl. Ocean Res.* 142, 103813. doi:10.1016/j.apor.2023.103813

Dialyna, E., and Tsoutsos, T. (2021). Wave energy in the mediterranean sea: resource assessment, deployed wecs and prospects. *Energies* 14, 4764. doi:10.3390/en14164764

ECMWF (2023). Ecmwf datasets. Accessed on: May 03, 2023.

Engwirda, D. (2014). Locally optimal delaunay-refinement and optimisation-based mesh generation. PhD thesis. Sydney, Australia: The University of Sydney.

Falcão, A. F., and Henriques, J. C. (2014). Model-prototype similarity of oscillating-water-column wave energy converters. *Int. J. Mar. Energy* 6, 18–34. doi:10.1016/j.ijome.2014.05.002

Ferrari, F., Besio, G., Cassola, F., and Mazzino, A. (2020). Optimized wind and wave energy resource assessment and offshore exploitability in the mediterranean sea. *Energy* 190, 116447. doi:10.1016/j.energy.2019.116447

Foteinis, S. (2022). Wave energy converters in low energy seas: current state and opportunities. *Renew. Sustain. Energy Rev.* 162, 112448. doi:10.1016/j.rser.2022.112448

Fournier, C., Pantoja, C., Resio, D., and Scott, D. (2004). "The development of a 40 year wave climate for the entire chilean coastline," in *Coastal structures 2003*, 689–701.

Freeman, M., Rose, D., Copping, A., Garavelli, L., and Hemery, L. (2024). From science to consenting: environmental effects of marine renewable energy

Gorr-Pozzi, E., García-Nava, H., Larrañaga, M., Jaramillo-Torres, M. G., and Verduzco-Zapata, M. G. (2021). Wave energy resource harnessing assessment in a subtropical coastal region of the pacific. *J. Mar. Sci. Eng.* 9, 1264. doi:10.3390/jmse9111264

Gunn, K., and Stock-Williams, C. (2012). Quantifying the global wave power resource. *Renew. Energy* 44, 296–304. doi:10.1016/j.renene.2012.01.101

Guo, C., Sheng, W., De Silva, D. G., and Aggidis, G. (2023). A review of the levelized cost of wave energy based on a techno-economic model. *Energies* 16, 2144. doi:10.3390/en16052144

Hersbach, H., Bell, B., Berrisford, P., Hirahara, S., Horányi, A., Muñoz-Sabater, J., et al. (2020). The era5 global reanalysis. *Q. J. R. Meteorological Soc.* 146, 1999–2049. doi:10.1002/qj.3803

Holthuijsen, L. H. (2010). *Waves in oceanic and coastal waters*. New York, United States: Cambridge University Press.

IMARES-UCR (2021). Data access consultancy. Accessed on: March 17, 2021.

INOCAR (2021). Instituto oceanografico y antartico de la armada de ecuador. Accessed on: January 19, 2021

Kamranzad, B., and Lin, P. (2020). Sustainability of wave energy resources in the south China sea based on five decades of changing climate. *Energy* 210, 118604. doi:10.1016/j.energy.2020.118604

Kumar, S., Baalisampang, T., Arzaghi, E., Garaniya, V., Abbassi, R., and Salehi, F. (2022). Synergy of green hydrogen sector with offshore industries: opportunities and challenges for a safe and sustainable hydrogen economy. *J. Clean. Prod.* 135545doi, 135545. doi:10.1016/j.jclepro.2022.135545

Kumar, V. S., and Anoop, T. (2015). Wave energy resource assessment for the indian shelf seas. *Renew. Energy* 76, 212–219. doi:10.1016/j.renene.2014.11.034

Lavidas, G. (2020). Selection index for wave energy deployments (siwed): a near-deterministic index for wave energy converters. *Energy* 196, 117131. doi:10.1016/j.energy.2020.117131

Lavidas, G., and Venugopal, V. (2017a). A 35 year high-resolution wave atlas for nearshore energy production and economics at the aegean sea. *Renew. Energy* 103, 401–417. doi:10.1016/j.renene.2016.11.055

Lavidas, G., and Venugopal, V. (2017b). Wave energy resource evaluation and characterisation for the libyan sea. *Int. J. Mar. energy* 18, 1–14. doi:10.1016/j.ijome.2017.03.001

Lavidas, G., Venugopal, V., and Friedrich, D. (2017). Wave energy extraction in scotland through an improved nearshore wave atlas. *Int. J. Mar. Energy* 17, 64–83. doi:10.1016/j.ijome.2017.01.008

Law-Chune, S., Aouf, L., Dalphinet, A., Levier, B., Drillet, Y., and Drevillon, M. (2021). Waverys: a cmems global wave reanalysis during the altimetry period. *Ocean. Dyn.* 71, 357–378. doi:10.1007/s10236-020-01433-w

Lehmann, M., Karimpour, F., Goudey, C. A., Jacobson, P. T., and Alam, M.-R. (2017). Ocean wave energy in the United States: current status and future perspectives. *Renew. Sustain. Energy Rev.* 74, 1300–1313. doi:10.1016/j.rser.2016.11.101

Lemenkova, P. (2019). Geophysical modelling of the middle America trench using gmt. *Ann. Valahia Univ. Targoviste. Geogr. Ser.* 19, 73–94. doi:10.2478/avutgs-2019-0008

Lin, J., Peng, W., Jiang, J., and Wang, L. (2024). Cost-effectively laboratory experimental techniques for performance assessment of scale-down wave energy converters. *Ocean. Eng.* 297, 117061. doi:10.1016/j.oceaneng.2024.117061

Liu, J., Meucci, A., Liu, Q., Babanin, A. V., Ierodiaconou, D., Xu, X., et al. (2023). A high-resolution wave energy assessment of south-east Australia based on a 40-year hindcast. *Renew. Energy* 215, 118943. doi:10.1016/j.renene.2023.118943

LLC, M. (2020). Gebco bathymetric compilation group 2019. gebco web map service.

Lucero, F., Catalán, P. A., Ossandón, Á., Beyá, J., Puelma, A., and Zamorano, L. (2017). Wave energy assessment in the central-south coast of Chile. *Renew. Energy* 114, 120–131. doi:10.1016/j.renene.2017.03.076

Martić, I., Degiuli, N., and Grlj, C. G. (2024). Scaling of wave energy converters for optimum performance in the adriatic sea. *Energy* 294, 130922. doi:10.1016/j.energy.2024.130922

Martinez, A., and Iglesias, G. (2020). Wave exploitability index and wave resource classification. *Renew. Sustain. Energy Rev.* 134, 110393. doi:10.1016/j.rser.2020.110393

Mazzaretto, O. M., Lucero, F., Besio, G., and Cienfuegos, R. (2020). Perspectives for harnessing the energetic persistent high swells reaching the coast of Chile. *Renew. Energy* 159, 494–505. doi:10.1016/j.renene.2020.05.031

Mazzaretto, O. M., and Menendez, M. (2024). A worldwide coastal analysis of the climate wave systems. *Front. Mar. Sci.* 11, 1385285. doi:10.3389/fmars.2024.1385285

Mediavilla, D. G., and Sepúlveda, H. H. (2016). Nearshore assessment of wave energy resources in central Chile (2009–2010). *Renew. energy* 90, 136–144. doi:10.1016/j.renene.2015.12.066

Medina, G. G., Yang, Z., Li, N., Cheung, K. F., and Lutu-McMoore, E. (2023). Wave climate and energy resources in American Samoa from a 42-year high-resolution hindcast. *Renew. Energy* 210, 604–617. doi:10.1016/j.renene.2023.03.031

Mentaschi, L., Kakoulaki, G., Vousdoukas, M., Voukouvalas, E., Feyen, L., and Besio, G. (2018). Parameterizing unresolved obstacles with source terms in wave modeling: a real-world application. *Ocean. Model.* 126, 77–84. doi:10.1016/j.ocemod.2018.04.003

Mentaschi, L., Pérez, J., Besio, G., Mendez, F., and Menendez, M. (2015). Parameterization of unresolved obstacles in wave modelling: a source term approach. *Ocean. Model.* 96, 93–102. doi:10.1016/j.ocemod.2015.05.004

Mentaschi, L., Vousdoukas, M., Besio, G., and Feyen, L. (2019). alphabetalab: automatic estimation of subscale transparencies for the unresolved obstacles source term in ocean wave modelling. *SoftwareX* 9, 1–6. doi:10.1016/j.softx.2018.11.006

Mork, G., Barstow, S., Kabuth, A., and Pontes, M. T. (2010). Assessing the global wave energy potential. *Int. Conf. Offshore Mech. Arct. Eng.* 49118, 447–454. doi:10.1115/OMAE2010-20473

NOAA (2021). National data buoy center. Accessed on: January 14, 2021.

NWS-NOAA (2021). Wavewatch iii model data access.

Perez, J., Menendez, M., and Losada, I. J. (2017). Gow2: a global wave hindcast for coastal applications. *Coast. Eng.* 124, 1–11. doi:10.1016/j.coastaleng.2017.03.005

Portilla-Yandun, J., and Guachamin-Acero, W. (2023). "Wave spectral analysis for designing wave energy converters," in Proceedings of the European Wave and Tidal Energy Conference, Bilbao, Spain, 3rd– 7th September 2023, 15. doi:10.36688/ewtec-2023-175

Portilla-Yandún, J., Salazar, A., Sosa, J., Latandret, S., and Cavaleri, L. (2020). Modeling multiple wave systems in the eastern equatorial pacific. *Ocean. Dyn.* 70, 977–990. doi:10.1007/s10236-020-01370-8

Raghavan, V., Simonetti, I., Metrikine, A. V., Lavidas, G., and Cappietti, L. (2024). A new numerical modelling framework for fixed oscillating water column wave energy conversion device combining bem and cfd methods: validation with experiments. *Ocean. Eng.* 301, 117543. doi:10.1016/j.oceaneng.2024.117543

Rascle, N., and Ardhuin, F. (2013). A global wave parameter database for geophysical applications. part 2: model validation with improved source term parameterization. *Ocean. Model.* 70, 174–188. doi:10.1016/j.ocemod.2012.12.001

Rasool, S., Muttaqi, K. M., Sutanto, D., and Hemer, M. (2022). Quantifying the reduction in power variability of co-located offshore wind-wave farms. *Renew. Energy* 185, 1018–1033. doi:10.1016/j.renene.2021.12.120

Rinaldi, G., Portillo, J., Khalid, F., Henriques, J., Thies, P., Gato, L., et al. (2018). Multivariate analysis of the reliability, availability, and maintainability characterizations of a spar–buoy wave energy converter farm. *J. Ocean Eng. Mar. Energy* 4, 199–215. doi:10.1007/s40722-018-0116-z

Rogers, W. E., Babanin, A. V., and Wang, D. W. (2012). Observation-consistent input and whitecapping dissipation in a model for wind-generated surface waves: description and simple calculations. *J. Atmos. Ocean. Technol.* 29, 1329–1346. doi:10.1175/jtech-d-11-00092.1

Rusu, L., and Onea, F. (2017). The performance of some state-of-the-art wave energy converters in locations with the worldwide highest wave power. *Renew. Sustain. Energy Rev.* 75, 1348–1362. doi:10.1016/j.rser.2016.11.123

Saha, S., Moorthi, S., Pan, H.-L., Wu, X., Wang, J., Nadiga, S., et al. (2010). The ncep climate forecast system reanalysis. *Bull. Am. Meteorological Soc.* 91, 1015–1058. doi:10.1175/2010bams3001.1

Saha, S., Moorthi, S., Wu, X., Wang, J., Nadiga, S., Tripp, P., et al. (2014). The ncep climate forecast system version 2. *J. Clim.* 27, 2185–2208. doi:10.1175/jcli-d-12-00823.1

Salvador, S., and Ribeiro, M. C. (2023). Socio-economic, legal, and political context of offshore renewable energies. *Wiley Interdiscip. Rev. Energy Environ.* 12, e462. doi:10.1002/wene.462

Schmitt, P., and Elsäßer, B. (2017). The application of froude scaling to model tests of oscillating wave surge converters. *Ocean. Eng.* 141, 108–115. doi:10.1016/j.oceaneng.2017.06.003

Shadman, M., Roldan-Carvajal, M., Pierart, F. G., Haim, P. A., Alonso, R., Silva, C., et al. (2023). A review of offshore renewable energy in south America: current status and future perspectives. *Sustainability* 15, 1740. doi:10.3390/su15021740

Sheng, W., Alcorn, R., and Lewis, A. (2014). Assessment of primary energy conversions of oscillating water columns. i. hydrodynamic analysis. *J. Renew. Sustain. Energy* 6. doi:10.1063/1.4896850

Soomere, T., and Eelsalu, M. (2014). On the wave energy potential along the eastern baltic sea coast. *Renew. energy* 71, 221–233. doi:10.1016/j.renene.2014.05.025

Soukissian, T., O'Hagan, A. M., Azzellino, A., Boero, F., Brito e Melo, A., Comiskey, P., et al. (2023). European offshore renewable energy: towards a sustainable future

Tawn, R., and Browell, J. (2022). A review of very short-term wind and solar power forecasting. *Renew. Sustain. Energy Rev.* 153, 111758. doi:10.1016/j.rser.2021.111758

Taylor, K. E. (2001). Summarizing multiple aspects of model performance in a single diagram. *J. Geophys. Res. Atmos.* 106, 7183–7192. doi:10.1029/2000JD900719

Tolman, H. L. (2009). User manual and system documentation of wavewatch iii tm version 3.14. *Tech. note, MMAB Contrib.*, 276.

UAIP-MARN (2021). Unidad de acceso a la informacion publica. Accessed on: February 03, 2021.

UN (2022). *Sustainable development goals progress report 2022. sdg report. Economic and Social Council*, 14–15.

Vanegas-Cantarero, M. M., Pennock, S., Bloise-Thomaz, T., Jeffrey, H., and Dickson, M. J. (2022). Beyond lcoe: a multi-criteria evaluation framework for offshore renewable energy projects. *Renew. Sustain. Energy Rev.* 161, 112307. doi:10.1016/j.rser.2022.112307

Ventura, Y., Rodriguez, Y., Odériz, I., Chavez, V., Mori, N., Felix, A., et al. (2022). New assessment of wave energy in relation to geomorphological and demographic characteristics on the pacific coast of baja California, Mexico. *Front. Mar. Sci.* 9, 872707. doi:10.3389/fmars.2022.872707

Vieira, M., Macedo, A., Alvarenga, A., Lafoz, M., Villalba, I., Blanco, M., et al. (2024). What future for marine renewable energy in Portugal and Spain up to 2030? forecasting plausible scenarios using general morphological analysis and clustering techniques. *Energy Policy* 184, 113859. doi:10.1016/j.enpol.2023.113859

Wan, Z., Su, Y., Li, Z., Zhang, X., Zhang, Q., and Chen, J. (2023). Analysis of the impact of suez canal blockage on the global shipping network. *Ocean & Coast. Manag.* 245, 106868. doi:10.1016/j.ocecoaman.2023.106868

Waters, R. (2008). *Energy from ocean waves: full scale experimental verification of a wave energy converter*. Electricity: Uppsala University. Ph.D. thesis.

Wessel, P., and Smith, W. H. (1996). A global, self-consistent, hierarchical, high-resolution shoreline database. *J. Geophys. Res. Solid Earth* 101, 8741–8743. doi:10.1029/96jb00104

Wg, I. (2013). The physical science basis. *Contribution of working group I to the fifth assessment report of the intergovernmental panel on climate change* 1535.

Windt, C., Davidson, J., and Ringwood, J. V. (2021). Numerical analysis of the hydrodynamic scaling effects for the wavestar wave energy converter. *J. Fluids Struct.* 105, 103328. doi:10.1016/j.jfluidstructs.2021.103328

WorldBank (2014). Electric power consumption (kwh *per capita*).

WorldBank (2023). Total greenhouse gas emissions (kt of co2 equivalent).

WW3DG (2019) *User manual and system documentation of WAVEWATCH III version 6.07*, 333. NOAA/NWS/NCEP/MMAB Tech. Note. NOAA-EMC).

Zhai, Q., Li, T., and Liu, Y. (2021). Life cycle assessment of a wave energy converter: uncertainties and sensitivities. *J. Clean. Prod.* 298, 126719. doi:10.1016/j.jclepro.2021.126719

Zhao, Z., Holbrook, N. J., Oliver, E. C., Ballestero, D., and Vargas-Hernandez, J. M. (2020). Characteristic atmospheric states during mid-summer droughts over central America and Mexico. *Clim. Dyn.* 55, 681–701. doi:10.1007/s00382-020-05283-6

Zheng, C.-w., Wu, D., Wu, H.-l., Guo, J., Shen, C., Tian, C., et al. (2022). Propagation and attenuation of swell energy in the pacific ocean. *Renew. Energy* 188, 750–764. doi:10.1016/j.renene.2022.02.071

Zieger, S., Babanin, A. V., Rogers, W. E., and Young, I. R. (2015). Observation-based source terms in the third-generation wave model wavewatch. *Ocean. Model.* 96, 2–25. doi:10.1016/j.ocemod.2015.07.014